


New graphical criterion for the selection of complete sets of polarization observables and its application to single-meson photoproduction as well as electroproduction

Y. Wunderlich ^{*}*Helmholtz-Institut für Strahlen- und Kernphysik, Universität Bonn, D-53115 Bonn, Germany*

(Received 24 June 2021; accepted 27 September 2021; published 25 October 2021)

This paper combines the graph-theoretical ideas behind Moravcsik's theorem with a completely analytic derivation of discrete phase ambiguities, recently published by Nakayama. The result is a new graphical procedure for the derivation of certain types of complete sets of observables for an amplitude-extraction problem with N helicity amplitudes. The procedure is applied to pseudoscalar meson photoproduction ($N = 4$ amplitudes) and electroproduction ($N = 6$ amplitudes), yielding complete sets with minimal length of $2N$ observables. For the case of electroproduction, this is the first time an extensive list of minimal complete sets is published. Furthermore, the generalization of the proposed procedure to processes with a larger number of amplitudes, i.e., $N > 6$ amplitudes, is sketched. The generalized procedure is outlined for the next more complicated example of two-meson photoproduction ($N = 8$ amplitudes).

DOI: [10.1103/PhysRevC.104.045203](https://doi.org/10.1103/PhysRevC.104.045203)

I. INTRODUCTION

Hadron spectroscopy is and has been a very important tool for the improvement of our understanding of nonperturbative QCD. Reactions among particles with spin have always been of central importance for spectroscopy. For the spectroscopy of baryons [1,2] in particular, most experimental activities in the recent years have taken place at facilities capable of measuring reactions induced by electromagnetic probes. Well-known experiments, all capable of measuring the photoproduction of one or several pseudoscalar mesons (as well as vector mesons), are the CBELSA/TAPS experiment at Bonn [3–8], CLAS at the Thomas Jefferson National Accelerator Facility (Newport News) [9–15], A2 at Mainz Microtron [16–24], and LEPS at SPring-8 (Hyōgo Prefecture) [25,26]. The GlueX Collaboration has started exploring completely new kinematic regimes for single-meson photoproduction recently [27–29]. Furthermore, new datasets on electroproduction have or will become available, measured by the CLAS-collaboration [30–33].

The currently accepted canonical method to determine physical properties of resonances (i.e., masses, widths and quantum numbers) from data are analyses using so-called energy-dependent (ED) partial-wave analysis models. Elaborate reaction-theoretic models are constructed in order to obtain the amplitude as a function of energy. Then, after fitting the data, the resulting amplitude is analytically continued into the complex energy-plane in order to search for the resonance poles. Well-known examples for such approaches are the Scattering Analysis Interactive Dial-in (SAID) analysis [34–38], the Bonn-Gatchina model [39–42], the Jülich-Bonn model [43–47], and the Mainz Unitary Isobar Model (MAID) analysis [48–51], among others.

In an approach that is complementary to the above-mentioned ED fits, one can ask for the maximal amount of information on the underlying reaction amplitudes that can be extracted from the data without introducing any model assumptions. One thus considers a generic *amplitude-extraction problem*, which is concerned with the extraction of N so-called spin amplitudes (often specified as helicity amplitudes H_i or transversity amplitudes b_i [52]) out of a set of N^2 polarization observables. Such an amplitude-extraction problem takes place at each point in the kinematical phase space individually. For a $2 \rightarrow 2$ reaction, this means at each point in energy and angle. For a $2 \rightarrow n$ reaction with $n \geq 3$ particles in the final state, the amplitude-extraction problem has to be solved in each higher-dimensional “bin” of phase space, where the phase space is spanned by $(3[2+n] - 10)$ independent kinematical variables [53]. In any case, the unknown overall phase can in principle have an arbitrary dependence on the full reaction kinematics.

For an ordinary scattering experiment such as the ones discussed in this work, the determination of the overall phase from data for a single reaction alone is a mathematical impossibility, due to the fact that observables are always bilinear Hermitean forms of the N amplitudes [54,55]. Alternative experiments have been proposed in the literature in order to remedy this problem: Goldberger and collaborators suggested a Hanbury-Brown and Twiss experiment to measure the overall phase [56], while Ivanov proposed to use Vortex beams in order to access information on the angular dependence of the overall phase [57]. However, both of these proposed methods cannot be realized experimentally at the time of this writing. The only alternative consists of the introduction of additional theoretical constraints. As many past studies on the mathematical physics of inverse scattering problems have shown [58–66], the unitarity of the S matrix is a very powerful constraint for restricting the overall phase. Unitarity constraints

^{*}Corresponding author: wunderlich@hiskp.uni-bonn.de

are of course inherent to many of the ED fit approaches mentioned above, since almost all of them are formulated for a simultaneous analysis of multiple coupled channels. However, within the context of an amplitude-extraction problem for *one* individual reaction, the overall phase cannot be determined, at least as long as the discussion remains fully model independent.

When confronted with a general amplitude-extraction problem, the question of minimizing the measurement effort leads one in a natural way to the search for so-called *complete experiments* [52,67] (or *complete sets of observables*). These are minimal subsets of the full set of N^2 observables that allow for an unambiguous extraction of the N amplitudes up to one overall phase. For an amplitude-extraction problem with an arbitrary number of amplitudes N , one can find the following compelling heuristic argument for the fact that at least $2N$ observables are required in order to determine the N amplitudes up to one unknown overall phase (cf. the introductions of Refs. [68,69], as well as footnote 1 in Ref. [70]). At least $2N - 1$ observables are needed in order to fix N moduli and $N - 1$ relative phases. However, with $2N - 1$ observables, there generally still remain so-called *discrete ambiguities* [52,71]. The resolution of these discrete ambiguities requires at least one additional observable. In this way, one obtains a minimum number of $2N$ observables. This heuristic argument of course tells nothing about *how* these $2N$ observables have to be selected. This is then the subject of works like the present one.

The minimal number of $2N$ has indeed turned out to be true for the specific reactions we found treated in the literature. For pion-nucleon scattering ($N = 2$), the argument demonstrating that indeed all four accessible observables have to be measured is still quite simple (cf. Ref. [69] as well as the introduction of Ref. [72]). The process of pseudoscalar meson photoproduction ($N = 4$) has been treated at length in the literature. Based on earlier results by Keaton and Workman [70,71], Chiang and Tabakin found in a seminal work [52] that 8 carefully selected observables can constitute a minimal complete set for this process. The result by Chiang and Tabakin has recently been substantiated in a rigorous algebraic proof by Nakayama [73], where all the discrete phase ambiguities implied by quite arbitrary selection patterns of observables were derived and the conditions for the resolution of these ambiguities were clearly stated. Some of Nakayama's derivations will also turn out to be important for this work. For pseudoscalar meson electroproduction ($N = 6$), the construction of some complete sets with 12 observables has been outlined by Tiator and collaborators [74], but an extensive list of complete sets has not been given in the latter reference. This is something that will be improved on in the present work. Finally, the process of two-meson photoproduction ($N = 8$) has been treated as well in some quite explicit works [75,76]. The complete sets for this process indeed have a minimal length of 16 [76].

In mathematical treatments of complete experiments such as the ones mentioned up to this point, one always assumes the observables to have vanishing measurement uncertainty. Once the mathematically “exact” complete sets have been established in this way, one can study the influence of nonva-

nishing measurement-uncertainties using high-level statistical methods. This has been done in a number of recent works by Ireland [77] and the Ghent group [78–80].

An interesting alternative approach for the deduction of complete sets of observables is given by Moravcsik's theorem [68]. This theorem has been reexamined in a recent work [69], where it has received slight corrections for the case of an odd number of amplitudes N . The theorem is formulated in the language of a “geometrical analog” [68], which yields a useful representation of complete sets in the shape of graphs. The advantages of the theorem are that it can be applied directly to any amplitude-extraction problem irrespective of N . Furthermore, it can be fully automated on a computer. However, the approach also has its drawbacks: For larger N (i.e., $N > 6$) [75,76,81,82], the number of relevant graph-topologies grows very rapidly, as $(N - 1)!/2$ [69]. This alone makes the computations quite expensive for more involved amplitude-extraction problems. Another drawback of (the modified form of) Moravcsik's theorem consists of the fact that for $N \geq 4$, the derived complete sets do not have the minimal length $2N$ any more, but are rather slightly over-complete (see in particular Sec. VII of Ref. [69]). The reason for the latter fact is that Moravcsik directly considered just the bilinear products $b_i^* b_j$ of amplitudes. However, polarization observables for $N \geq 4$ generally are invertible linear combinations of such bilinear products.

The present work is an attempt to devise an approach similar to (the modified form of) Moravcsik's theorem [69], but which can get the length of the derived complete sets down to $2N$, for amplitude-extraction problems with $N \geq 4$. Generally, the proposed approach can be applied to any amplitude-extraction problem with an *even* number of amplitudes N . In order to achieve this, we combine the graph-theoretical ideas according to Refs. [68,69] with the results derived by Nakayama [73] for the discrete phase ambiguities implied by selections of pairs of observables. Although these ambiguities have been originally derived by Nakayama for photoproduction [73], we get a criterion that directly facilitates deriving minimal complete sets for electroproduction as well. A crucial new ingredient for the procedure proposed in this work is that the graphs have to be imbued with additional directional information. The graphical criterion formulated in this work, together with the types of graphs needed for it, are to our knowledge new.

This paper is organized as follows. The new graphical criterion is motivated and deduced in Sec. II, as a result of the combination of the ideas behind Moravcsik's theorem and the phase ambiguities as derived by Nakayama [73]. We then illustrate the new criterion in applications to single-meson photo- and electroproduction in Secs. III and IV. Some ideas on the generalization of the proposed procedure to problems with a larger number of $N > 6$ amplitudes are stated in Sec. V, which is followed by the conclusion in Sec. VI. Three Appendices collect a review of the recently published modified form of Moravcsik's theorem [69], as well as lengthy calculations which are however of vital importance for the present work. Elaborate lists of the newly derived complete sets for electroproduction can be found in the Supplemental Material [83].

II. THE NEW GRAPHICAL CRITERION

In this section, the new graphical criterion for complete sets of observables is derived deductively. It is based on a combination of the graph-theoretical ideas from Moravcsik's theorem [68,69], where each complete sets of observables has a lucid representation in terms of a graph, and recent derivations of discrete phase ambiguities given in full detail by Nakayama [73]. Since Moravcsik's theorem serves as a useful reference point to the new ideas developed in this section, and also to keep this work self-contained, a review of a recently published slightly modified version of the theorem is given in Appendix A. In this Appendix, also some pictorial examples for complete graphs according to Moravcsik can be found.

We start with the standard assumption that the moduli $|b_i|$ of the N amplitudes b_1, \dots, b_N have already been determined from a set of N diagonal observables (cf. Appendix A and Refs. [52,68,69,73]). Consider now a so-called (nondiagonal) *shape class* composed of four observables, which is a mathematical structure that repeatedly appears in the problems of single-meson photoproduction and electroproduction (cf. Tables I and III). The four observables belonging to the shape class, which we denote by the superscript "n," are given by the following linear combinations of bilinear amplitude products (the notation for the observables is taken over from Ref. [73]):

$$\begin{aligned} \mathcal{O}_{1+}^n &= \text{Im}[b_j^* b_i + b_l^* b_k] \\ &= |b_i||b_j| \sin \phi_{ij} + |b_k||b_l| \sin \phi_{kl}, \end{aligned} \quad (1)$$

$$\begin{aligned} \mathcal{O}_{1-}^n &= \text{Im}[b_j^* b_i - b_l^* b_k] \\ &= |b_i||b_j| \sin \phi_{ij} - |b_k||b_l| \sin \phi_{kl}, \end{aligned} \quad (2)$$

$$\begin{aligned} \mathcal{O}_{2+}^n &= \text{Re}[b_j^* b_i + b_l^* b_k] \\ &= |b_i||b_j| \cos \phi_{ij} + |b_k||b_l| \cos \phi_{kl}, \end{aligned} \quad (3)$$

$$\begin{aligned} \mathcal{O}_{2-}^n &= \text{Re}[b_j^* b_i - b_l^* b_k] \\ &= |b_i||b_j| \cos \phi_{ij} - |b_k||b_l| \cos \phi_{kl}. \end{aligned} \quad (4)$$

The four indices $i, j, k, l \in 1, \dots, N$ (for either $N = 4$ in case of photoproduction or $N = 6$ for electroproduction) have to be all pairwise distinct. In this way, every shape class composed of four observables, which has the above-given structure, is in one-to-one correspondence to a particular pair of relative phases $\{\phi_{ij}, \phi_{kl}\}$. In the case of photoproduction ($N = 4$, Sec. III), one has three shape classes of this type, while for electroproduction ($N = 6$, Sec. IV), one encounters seven such shape classes, containing four observables each.

A shape class composed of four observables such as in Eqs. (1)–(4) really represents the *simplest nontrivial example* of such a class, since any simpler combination of bilinear amplitude products would just amount to the real and imaginary parts of the products $b_j^* b_i$ themselves, without any additional linear combination (cf. discussions in Appendix A). For problems with $N > 6$ amplitudes, one generally encounters more involved shape classes (cf. Sec. V).

Before discussing the discrete phase ambiguities implied by different selections of observables picked from the shape class given in Eqs. (1)–(4), we need to introduce another

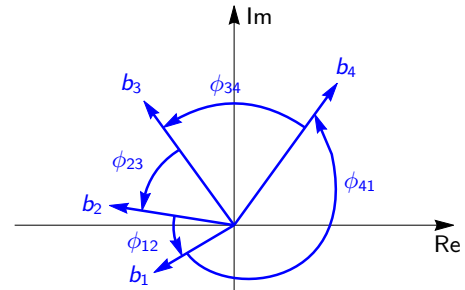


FIG. 1. The general consistency relation (5) is illustrated for the example of an amplitude-extraction problem with $N = 4$ amplitudes b_1, \dots, b_4 . The relation one deduces geometrically from the given diagram is $\phi_{12} + \phi_{23} + \phi_{34} + \phi_{41} = 2\pi$, which up to addition of 2π is equivalent to $\phi_{12} + \phi_{23} + \phi_{34} + \phi_{41} = 0$.

important part of the proofs yet to be presented, which is given by so-called *consistency relations* [69,73]. In case the *connectedness criterion* is fulfilled by the graphs that represent potentially complete sets of observables (cf. discussions further below in this section and in Appendix A), one can establish a consistency relation among all the occurring relative phases, which generally takes the shape:¹

$$\phi_{1i} + \phi_{ij} + \dots + \phi_{kl} = 0. \quad (5)$$

The pairings of indices in relative phases occurring in this relation is in one-to-one correspondence to the considered graph topology. The consistency relation (5) is a natural constraint for an arrangement of N amplitudes in the complex plane (cf. the illustration in Fig. 1) and any valid solution of the considered amplitude-extraction problem has to satisfy it. It will turn out to be important for this work to fix a standard convention for writing down consistency relations: We want to isolate all relative phases on one side of the equation sign [such as in Eq. (5)], want all relative phases to have a positive sign and want the index pairings in the appearing relative phases to correspond to a *definite direction of translation* (or just short: a *direction*) for the graph. The direction of translation is fixed by starting at amplitude point "1," then stepping through the graph along direct connections of amplitudes which have to be in one-to-one correspondence to the sequence of indices appearing in Eq. (5), until ending up again at amplitude point "1." This convention will turn out to be important for the discussion from here on.

Consistency relations such as (5) are crucial for the derivation of fully complete sets. A selection of observables picked from several copies of the above-given shape class, with the selection corresponding to a particular considered graph, leads to a set of \mathcal{N}_{amb} potentially ambiguous solutions.² For each of

¹The consistency relation (5), as well as all other relations among phases appearing in this work, is only valid up to addition of multiples of 2π .

²For the ambiguities of real and imaginary parts of bilinear products $b_j^* b_i$ considered in case of Theorem 2 in Appendix A, the discrete phase ambiguities are always twofold for each relative phase individually and thus one always has $\mathcal{N}_{\text{amb}} = 2^N$. For the selections

these \mathcal{N}_{amb} discrete phase ambiguities, one can write down a consistency relation, where the respective ambiguous solutions are labeled by a corresponding superscript- λ on the relative phases:

$$\phi_{li}^\lambda + \phi_{ij}^{\lambda'} + \dots + \phi_{kl}^{\lambda^{(n)}} = 0. \quad (6)$$

The criteria stated in Theorem 1 derived in this section, as well as Theorem 2 from Appendix A, are now the results of a careful analysis of all possible cases where no degeneracies³ occur any more among the \mathcal{N}_{amb} possible relations (6) (see also Appendix A of Ref. [69] for a more detailed derivation of Theorem 2). The only difference is that Theorem 2 is only valid in the basis of fully *decoupled* bilinear products $b_j^* b_i$, while Theorem 1 to be deduced below holds for selections of observables from the nondecoupled shape class given in Eqs. (1) to (4). In case all degeneracies are indeed resolved (in case of either Theorem 1 or Theorem 2), full completeness is obtained and the solution of the amplitude-extraction problem is thus unique.

We now proceed to enumerate the discrete ambiguities for the relative phases implied by the selection of any pair of observables from the four quantities (1) to (4). A full derivation of these ambiguities has been given by Nakayama [73], based on earlier ideas by Chiang and Tabakin [52]. In the following, we only cite the results. A full derivation according to Nakayama is outlined in more detail in Appendix B, in order to keep the present work self-contained.

One does not need any elaborate additional derivations in case the pair of observables is selected in such a way that the bilinear amplitude products fully *decouple*. This is also the case in which Theorem 2 from Appendix A can be directly used, i.e., the case of the two following possible selections (see also Ref. [73]):

A.1 ($\mathcal{O}_{1+}^n, \mathcal{O}_{1-}^n$):

This particular selection of observables allows for the isolation of both sines of the relative phases ϕ_{ij} and ϕ_{kl} , according to the following linear combinations of observables:

$$\sin \phi_{ij} = \frac{\mathcal{O}_{1+}^n + \mathcal{O}_{1-}^n}{2|b_i||b_j|}, \quad \sin \phi_{kl} = \frac{\mathcal{O}_{1+}^n - \mathcal{O}_{1-}^n}{2|b_k||b_l|}. \quad (7)$$

In this way, one obtains a discrete sine-type ambiguity for the two relative phases [cf. Eq. (A6)]:

$$\phi_{ij}^\lambda = \phi_{ij}^\pm = \begin{cases} +\alpha_{ij}, \\ \pi - \alpha_{ij}, \end{cases} \quad \phi_{kl}^{\lambda'} = \phi_{kl}^\pm = \begin{cases} +\alpha_{kl}, \\ \pi - \alpha_{kl}, \end{cases} \quad (8)$$

of observables from the nondiagonal shape class considered in this section, \mathcal{N}_{amb} may differ from 2^N .

³Two equations from the \mathcal{N}_{amb} possibilities (6) are called *degenerate* in case they can be transformed into each other using the following two operations [69,76]:

- (i) multiplication of the whole equation by (-1) ,
- (ii) addition (and/or subtraction) of multiples of 2π .

where the values of the two selected observables uniquely fix both α_{ij} and α_{kl} on the interval $[-\pi/2, \pi/2]$. Since both λ and λ' in Eq. (8) can take their values \pm independently, the discrete ambiguity is fourfold.

A.2 ($\mathcal{O}_{2+}^n, \mathcal{O}_{2-}^n$):

For this particular selection of observables, one obtains an isolation of the cosines according to:

$$\cos \phi_{ij} = \frac{\mathcal{O}_{2+}^n + \mathcal{O}_{2-}^n}{2|b_i||b_j|}, \quad \cos \phi_{kl} = \frac{\mathcal{O}_{2+}^n - \mathcal{O}_{2-}^n}{2|b_k||b_l|}. \quad (9)$$

This leads to discrete cosine-type ambiguities for the two relative phases ϕ_{ij} and ϕ_{kl} [cf. Eq. (A4)]:

$$\phi_{ij}^\lambda = \phi_{ij}^\pm = \begin{cases} +\alpha_{ij}, \\ -\alpha_{ij}, \end{cases} \quad \phi_{kl}^{\lambda'} = \phi_{kl}^\pm = \begin{cases} +\alpha_{kl}, \\ -\alpha_{kl}, \end{cases} \quad (10)$$

with α_{ij} and α_{kl} both fixed uniquely on the interval $[0, \pi]$, from the values of the two selected observables. The discrete phase ambiguity is again fourfold (due to $\lambda, \lambda' = \pm$).

Once a ‘‘crossed’’ pair of observables, i.e., with one observable chosen from $\mathcal{O}_{1\pm}^n$ and the other one from $\mathcal{O}_{2\pm}^n$ is selected, the elaborate derivations outlined in Appendix B become necessary. These are, however, also the selections which are much more interesting and important for the graphical criterion proposed in this work. One has to distinguish the following four cases [73]:

B.1. ($\mathcal{O}_{1+}^n, \mathcal{O}_{2+}^n$):

For this selection of observables, one only obtains a twofold discrete phase ambiguity. Only the following two possible pairs of values are allowed for the relative phases ϕ_{ij} and ϕ_{kl} (see Ref. [73] and Appendix B):⁴

$$\begin{cases} \phi_{ij} = -\zeta + \alpha_{ij}, \\ \phi_{kl} = -\zeta - \alpha_{kl} + \pi, \end{cases} \quad \text{or} \quad \begin{cases} \phi_{ij} = -\zeta - \alpha_{ij} + \pi, \\ \phi_{kl} = -\zeta + \alpha_{kl}, \end{cases} \quad (11)$$

where both α_{ij} and α_{kl} are uniquely fixed on the interval $[-\pi/2, \pi/2]$ via the values of the selected pair of observables (cf. Eqs. (B9) and (B11) in Appendix B).

The quantity ζ in the definition of this twofold ambiguity (11) is the new ingredient which appears in case of a selection of a crossed pair of observables. As defined in Ref. [73], this quantity ζ is equal to the polar angle in a two-dimensional coordinate system, where \mathcal{O}_{1+}^n defines the x coordinate and \mathcal{O}_{2+}^n

⁴The expressions for the ambiguities (11) to (14), as derived in Appendix B, are formally a bit different compared to those of Ref. [73]. However, the most important features of the derived ambiguities (i.e., the signs of the ζ angles) remain the same and therefore the statements of Theorem 1 developed in this section do not change, no matter which formulas one uses. In order to keep the present work self-contained, we stick to the expressions for the ambiguities as derived in Appendix B.

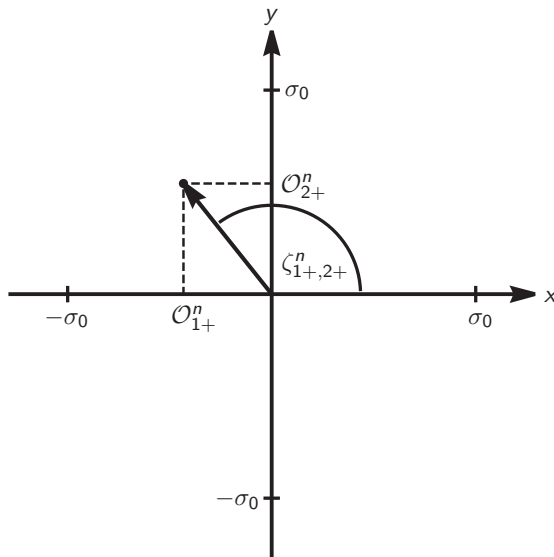


FIG. 2. The meaning of the angle $\zeta \equiv \zeta_{1+,2+}^n$ is illustrated. This picture directly corresponds to the definitions (B4) and (B5) in Appendix B. The modulus of the value for each observable (O_{1+}^n, O_{2+}^n) is limited by the unpolarized differential cross section σ_0 of the considered process.

the y coordinate (see Fig. 2). We therefore call it a “transitional angle.” This angle should actually be denoted as “ $\zeta_{1+,2+}^n$ ” since it depends on the values of the selected pair of observables (cf. Appendix B and Ref. [73]). However, in order to keep the notation as simple as possible, we only write ζ (and ζ', ζ'', \dots for any additional transitional angles that appear in an equation). The transitional angles are of vital importance for the resolution of degenerate consistency relations⁵ and therefore also for the removal of phase ambiguities (cf. Ref. [73]). They are therefore the *central objects of interest* for our proposed graphical criterion.

B.2. (O_{1+}^n, O_{2-}^n):

In this case, one obtains the twofold discrete phase ambiguity (cf. Appendix B)

$$\begin{cases} \phi_{ij} = -\zeta + \alpha_{ij}, \\ \phi_{kl} = \zeta - \alpha_{kl}, \end{cases} \quad \text{or} \quad \begin{cases} \phi_{ij} = -\zeta - \alpha_{ij} + \pi, \\ \phi_{kl} = \zeta + \alpha_{kl} - \pi, \end{cases} \quad (12)$$

where the values of the selected pair of observables uniquely fix both α_{ij} and α_{kl} on the interval

⁵We note here that special values for the ζ angle exist where it may generally lose its ability to resolve degenerate consistency relations, namely $\zeta = 0, \frac{\pi}{2}, \pi, \frac{3\pi}{2}, 2\pi$, and multiples thereof. Considering Fig. 2, we see that these values occur when at least one observable in the pair (O_{1+}^n, O_{2+}^n) vanishes. These special configurations belong to the surfaces of vanishing measure in the parameter space, on which Theorem 1 can lose its validity (cf. comments made at the end of Sec. II, as well as similar discussions in Ref. [73]). In the present work, we disregard such special cases.

$[-\pi/2, \pi/2]$ (see Eqs. (B28) and (B29) in Appendix B), as well as the value of the transitional angle

$$\zeta \equiv \zeta_{1+,2-}^n.$$

B.3. (O_{1-}^n, O_{2+}^n):

For this selection of observables, one obtains the twofold discrete phase ambiguity (see Appendix B)

$$\begin{cases} \phi_{ij} = -\zeta + \alpha_{ij}, \\ \phi_{kl} = \zeta + \alpha_{kl} - \pi, \end{cases} \quad \text{or} \quad \begin{cases} \phi_{ij} = -\zeta - \alpha_{ij} + \pi, \\ \phi_{kl} = \zeta - \alpha_{kl}, \end{cases} \quad (13)$$

where both α_{ij} and α_{kl} are uniquely fixed on the interval $[-\pi/2, \pi/2]$ from the values of the selected pair of observables (cf. Eqs. (B38) and (B39) in Appendix B). The selected observables also fix the transitional angle $\zeta \equiv \zeta_{1-,2+}^n$.

B.4. (O_{1-}^n, O_{2-}^n):

This selection of observables implies the twofold discrete phase ambiguity (cf. Appendix B)

$$\begin{cases} \phi_{ij} = -\zeta + \alpha_{ij}, \\ \phi_{kl} = -\zeta + \alpha_{kl}, \end{cases} \quad \text{or} \quad \begin{cases} \phi_{ij} = -\zeta - \alpha_{ij} + \pi, \\ \phi_{kl} = -\zeta - \alpha_{kl} + \pi, \end{cases} \quad (14)$$

where the values of the selected pair of observables uniquely fix both α_{ij} and α_{kl} on the interval $[-\pi/2, \pi/2]$ (see Eqs. (B20) and (B21) in Appendix B) and furthermore also define the value of the transitional angle $\zeta \equiv \zeta_{1-,2-}^n$.

The key is now to observe that the sign of the transitional angle ζ does *not* change for each of the two relative phases, i.e., ϕ_{ij} or ϕ_{kl} , individually when passing from one ambiguous solution to the other one. This is true in all of the cases B.1, ..., B.4. The sign of ζ may however vary in a comparison *between* ϕ_{ij} and ϕ_{kl} .

Still, when evaluating all the different cases possible for a particular consistency relation (6), the ζ angles have a great power for resolving discrete ambiguities or equivalently for removing degenerate pairs of equations. Thus, one has to carefully keep track of the signs of the ζ 's appearing in Eqs. (11) to (14), when devising a graphical criterion.

There is another sign which is important: This has to do with the index structure of the relative phases, as they appear in our standard convention for the consistency relation (5) [or (6)]. For instance, in case ϕ_{ij} appears in this equation with reversed placement ϕ_{ji} , there appears yet another sign one has to carefully keep track of.

Our proposed graphical criterion is now, in essence, a way to keep track of both the above-mentioned signs, in such a way that at least one transitional ζ angle survives in all the possible cases for the consistency relation (6) (compare this to expressions given in Sec. III of Ref. [73]).

We always start with the standard assumption that N suitable observables have been measured in order to uniquely fix the N moduli $|b_1|, \dots, |b_N|$. For the selection of the remaining observables, which are supposed to uniquely fix all relative phases between the N amplitudes, the criterion reads as follows:

Theorem 1 (Proposed graphical criterion):

Start with one possible topology for a connected graph with N vertices of order two, i.e., with exactly two edges attached to each vertex. The vertices, or points, again represent the N amplitudes of the problem. The chosen graph has to have exactly N edges (or link lines) and furthermore has to satisfy in addition the following constraint:

- (i) The graph should be chosen in such a way that only those connections of amplitude points appear which are in direct correspondence to any pair of relative phases $\{\phi_{ij}, \phi_{kl}\}$ from a particular shape class of four observables. The graph is thus constructed to exactly match selections of observables from classes with the structure (1) to (4).

Now, select $N/2$ pairs of observables from the shape classes implied by the considered graph. The selection of $N/2$ pairs is the reason why the proposed approach can only be directly applied to problems with an *even* number of amplitudes N . Draw the following connections of points, based on the selection made:

- (i) In case the selection A.1 has been made, draw a single dashed line which connects the respective amplitude points (these are then two link lines, in this case). In case a pair of observables has been chosen according to A.2, draw the corresponding pair of link lines as single solid lines.
- (ii) In case any of the selections B.1, . . . , B.4 has been made, draw a double line for both connections of the corresponding amplitude points. In case multiple such pairs of double lines appear in the graph, draw a different style of double line for each different shape class (i.e., normal double line, wavy double line, dashed double line, dotted double line, . . .). This has to be done in order to keep track of relative phases fixed by different shape classes of observables.

Now, draw arrows into the N link lines which *indicate the direction of translation* through the graph, according to our standard convention of writing the consistency relation (5) [cf. comments below Eq. (5)]. We call these arrows “directional arrows.” The standard form of the consistency relation (5) would imply directional arrows pointing as follows: $1 \rightarrow i$, $i \rightarrow j$, . . . , $k \rightarrow 1$.

Then, draw an additional ζ -sign arrow next to each double line or, depending on the graphic layout, *into* the double line (cf. figures in Secs. III and IV). In case the considered double line corresponds to an arbitrary relative phase ϕ_{ab} , the ζ -sign arrow has to point from $a \rightarrow b$ in case the ζ angle appears with a *positive* sign in the ambiguity written in the corresponding case from B.1–B.4 (cf. the descriptions of the cases above). The ζ -sign arrow has to point from $b \rightarrow a$ in case the ζ angle appears with a *negative* sign in the equations defining the corresponding discrete phase ambiguity (cases B.1–B.4).

The graph constructed in this lengthy procedure, and therefore also the corresponding set of observables, allows for a unique solution of the amplitude-extraction problem if it

contains *at least one pair of double lines* and furthermore satisfies the following criterion:

- (C1) For *at least one of the pairs of double lines* in the thus constructed graph, one of the following two conditions has to be fulfilled for the graph to be fully complete (note that both conditions cannot be satisfied at the same time):
 - (i) for *both* double lines, the directional arrows have to point into the *same* direction as the corresponding ζ -sign arrows,
 - (ii) for *both* double lines, the directional arrows have to point into the direction *opposite* to the direction of the respective ζ -sign arrows.

The single dashed and solid lines are not really important any more for this criterion,⁶ as opposed to Theorem 2 from Appendix A.

As in the case of the modified form of Moravcsik’s theorem (Theorem 2 in Appendix A), the connectedness condition imposed on the graphs considered in our new graphical criterion directly removes any possibilities for continuous ambiguities. The remaining conditions stated in Theorem 1 above then are included solely for the purpose of resolving all possible remaining discrete phase ambiguities.

Both of the possible conditions stated in the criterion (C1) above make sure that the transitional ζ angle belonging to the corresponding pair of observables appears in all cases for the consistency relation (6) with always the *same sign*. This is a plus sign in case of the first condition mentioned in (C1), or a minus sign in case of the second condition. Therefore, in exactly these cases the transitional ζ angles do *not* cancel out. This automatically removes all possible degeneracies among the possible cases for the consistency relation (6). We will illustrate in more detail how this works in our treatment of the example case of single-meson photoproduction, in Sec. III.

We note that the above-stated criterion is only valid for the special case of a selection of exactly two observables from each shape class of four [cf. Eqs. (1) to (4)]. In the case of Nakayama’s work [73], which treated single-meson photoproduction, this was called the “(2+2)-case.” Certainly this specific assumption of choosing only pairs of observables from each shape class restricts the complete sets which we can derive to this certain particular subset and the full set of possible complete experiments is certainly larger. We do not want to exclude the possibility that the graphical criterion stated above may in the future be generalized to more general selections of observables (such as the “(2+1+1)-case” in Nakayama’s work [73]), but at present it does not cover such more general possibilities.

As in the case of Moravcsik’s theorem in its modified form (Theorem 2 from Appendix A), there do exist singular subsurfaces in the parameter-space composed of the relative phases, on which Theorem 1 as stated above loses its validity. Nakayama also mentioned such configurations in his

⁶The ζ angles have now taken the role of the “residual summands of π ” needed in the proof of Theorem 2 (see Appendix A of Ref. [69]).

TABLE I. The definitions of the 16 polarization observables in pseudoscalar meson photoproduction (cf. Ref. [52]) are collected here. The observables are written in terms of transversity amplitudes b_1, b_2, b_3, b_4 . The nondiagonal observables are given in Nakayama's symbolic notation $\mathcal{O}_{v\pm}^n$ (cf. Ref. [73]), but the ordinary names of the observables are given as well. The subdivision of the 16 observables into four shape classes is explicitly shown. Furthermore, for the three nondiagonal shape classes a, b , and c , the corresponding pairs of relative phases are indicated. The definitions and sign-conventions are chosen to be consistent with Ref. [55].

Observable	Relative phases	Shape class
$\sigma_0 = \frac{1}{2}(b_1 ^2 + b_2 ^2 + b_3 ^2 + b_4 ^2)$ $-\check{\Sigma} = \frac{1}{2}(b_1 ^2 + b_2 ^2 - b_3 ^2 - b_4 ^2)$ $-\check{T} = \frac{1}{2}(- b_1 ^2 + b_2 ^2 + b_3 ^2 - b_4 ^2)$ $\check{P} = \frac{1}{2}(- b_1 ^2 + b_2 ^2 - b_3 ^2 + b_4 ^2)$		$S = D$
$\mathcal{O}_{1+}^a = b_1 b_3 \sin \phi_{13} + b_2 b_4 \sin \phi_{24} = \text{Im}[b_3^* b_1 + b_4^* b_2] = -\check{G}$ $\mathcal{O}_{1-}^a = b_1 b_3 \sin \phi_{13} - b_2 b_4 \sin \phi_{24} = \text{Im}[b_3^* b_1 - b_4^* b_2] = \check{F}$ $\mathcal{O}_{2+}^a = b_1 b_3 \cos \phi_{13} + b_2 b_4 \cos \phi_{24} = \text{Re}[b_3^* b_1 + b_4^* b_2] = -\check{E}$ $\mathcal{O}_{2-}^a = b_1 b_3 \cos \phi_{13} - b_2 b_4 \cos \phi_{24} = \text{Re}[b_3^* b_1 - b_4^* b_2] = \check{H}$	$\{\phi_{13}, \phi_{24}\}$	$a = \mathcal{BT} = \text{PR}$
$\mathcal{O}_{1+}^b = b_1 b_4 \sin \phi_{14} + b_2 b_3 \sin \phi_{23} = \text{Im}[b_4^* b_1 + b_3^* b_2] = \check{O}_{z'}$ $\mathcal{O}_{1-}^b = b_1 b_4 \sin \phi_{14} - b_2 b_3 \sin \phi_{23} = \text{Im}[b_4^* b_1 - b_3^* b_2] = -\check{C}_{z'}$ $\mathcal{O}_{2+}^b = b_1 b_4 \cos \phi_{14} + b_2 b_3 \cos \phi_{23} = \text{Re}[b_4^* b_1 + b_3^* b_2] = -\check{C}_{z'}$ $\mathcal{O}_{2-}^b = b_1 b_4 \cos \phi_{14} - b_2 b_3 \cos \phi_{23} = \text{Re}[b_4^* b_1 - b_3^* b_2] = -\check{O}_{z'}$	$\{\phi_{14}, \phi_{23}\}$	$b = \mathcal{BR} = \text{AD}$
$\mathcal{O}_{1+}^c = b_1 b_2 \sin \phi_{12} + b_3 b_4 \sin \phi_{34} = \text{Im}[b_2^* b_1 + b_4^* b_3] = -\check{L}_{z'}$ $\mathcal{O}_{1-}^c = b_1 b_2 \sin \phi_{12} - b_3 b_4 \sin \phi_{34} = \text{Im}[b_2^* b_1 - b_4^* b_3] = -\check{T}_{z'}$ $\mathcal{O}_{2+}^c = b_1 b_2 \cos \phi_{12} + b_3 b_4 \cos \phi_{34} = \text{Re}[b_2^* b_1 + b_4^* b_3] = -\check{L}_{z'}$ $\mathcal{O}_{2-}^c = b_1 b_2 \cos \phi_{12} - b_3 b_4 \cos \phi_{34} = \text{Re}[b_2^* b_1 - b_4^* b_3] = \check{T}_{z'}$	$\{\phi_{12}, \phi_{34}\}$	$c = \mathcal{TR} = \text{PL}$

treatment of photoproduction [73]. However, such singular surfaces again have negligible measure and therefore we do not further consider such special cases in the present work.

Theorem 1 stated above allows for the graphical derivation of minimal complete sets of $2N$ observables for the cases of single-meson photoproduction ($N = 4$) and electroproduction ($N = 6$), which has not been possible using the modified form of Moravcsik's theorem as stated in Appendix A (see Ref. [69]). This fact will be illustrated in Secs. III and IV. In case one wishes to consider problems with a larger number of $N > 6$ amplitudes, new obstacles appear which mainly are connected to the fact that the shape classes encountered in these cases are more involved. We will comment on these issues in Sec. V.

III. APPLICATION TO PSEUDOSCALAR MESON PHOTOPRODUCTION ($N = 4$)

Pseudoscalar meson photoproduction is generally described by $N = 4$ complex amplitudes, which are accompanied by 16 polarization observables [52,73]. The definitions of these observables in terms of transversity amplitudes b_1, \dots, b_4 are given in Table I. There exist four shape classes of diagonal (D), right-parallelogram (PR), antidiagonal (AD) and left-parallelogram (PL) type (the importance of such shape classes was originally pointed out in Ref. [52]). Every shape class except for the class of diagonal observables (D) has the generic form given in Eqs. (1) to (4) and thus contains four observables. The diagonal shape class D contains the unpolarized differential cross section and the three single-spin observables $\check{\Sigma}$, \check{T} , and \check{P} . Each of the three nondiagonal shape classes is in exact correspondence to one of the three groups of beam-target (\mathcal{BT}), beam-recoil (\mathcal{BR}), and target-recoil (\mathcal{TR}) experiments, as indicated in Table I.

For the observables in the nondiagonal shape classes, we use the notation introduced by Nakayama [73], which has also been used already in Sec. II.

We mention here the fact that the 16 observables can be written as bilinear Hermitean forms defined in terms of a basis of 4×4 Dirac matrices $\check{\Gamma}^\alpha$, which have been introduced in Ref. [52] (see also Ref. [69]). We, however do not list these Dirac matrices explicitly in this work, although their internal structure is of course contained implicitly in all the mathematical facts leading to Theorem 1 of Sec. II. Furthermore, the name ‘‘shape class’’ actually stems from the shapes of these Dirac matrices [52,55].

We begin with the standard assumption that all four observables from the diagonal shape class (D) have been measured in order to uniquely fix the four moduli $|b_1|, \dots, |b_4|$. Therefore, the task is now to select four more observables from the remaining nondiagonal shape classes a, b , and c , which corresponds to the determination of complete sets with minimal length $2N = 8$, in order to uniquely specify the relative phases. This is where the criterion formulated in Theorem 1 of Sec. II becomes useful.

The problem with $N = 4$ amplitudes allows for three non-trivial basic topologies for a connected graph (or ‘‘closed loop’’) as demanded at the beginning of Theorem 1. The three topologies are shown in Fig. 3, where also a definite *direction of translation* is indicated for each graph. If we consider for example the first boxlike topology shown in Fig. 3, we see that the indicated direction of the graph is in one-to-one correspondence to the following standard convention for writing the consistency relation [see Eq. (5), as well as comments below that equation]:

$$I = (b, c): \phi_{12} + \phi_{23} + \phi_{34} + \phi_{41} = 0. \quad (15)$$

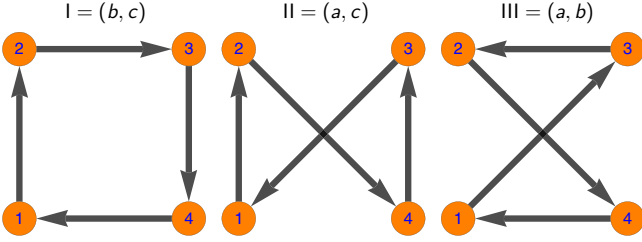


FIG. 3. The three possible start topologies for pseudoscalar meson photoproduction ($N = 4$ amplitudes) are drawn here. Each graph is drawn with a particular *direction*, which is intimately connected to our way of writing the corresponding consistency relation, i.e., Eqs. (15)–(17) (cf. comments made below Eq. (5) in Sec. II). Each topology corresponds to the relative phases from a particular combination of two shape classes (cf. Table I), as is indicated above the graphs (cf. discussion in the main text).

In exactly the same way, one can write a uniquely specified consistency relation for each of the remaining two topologies, with their respective direction of translation. For the second and third topology shown in Fig. 3, we have the expressions:

$$\text{II} = (a, c): \phi_{12} + \phi_{24} + \phi_{43} + \phi_{31} = 0, \quad (16)$$

$$\text{III} = (a, b): \phi_{13} + \phi_{32} + \phi_{24} + \phi_{41} = 0. \quad (17)$$

We again stress the fact that the sign-choices fixed in the standard conventions (15) to (17) are crucial for the applicability of the graphical criterion formulated in Theorem 1 of Sec. II.

As already indicated in the Eqs. (15) to (17) written above, one should note that each of the topologies shown in Fig. 3, as well as each of the consistency relations (15) to (17) is in direct correspondence to a particular combination of shape classes from which the pairs of observables are to be picked (cf. Table I). To be more precise, the first topology in Fig. 14 corresponds to the combination of shape classes (b, c) , the second topology relates to the combination (a, c) and the third topology corresponds to (a, b) .

We now consider some examples for (in-)complete graphs, in order to illustrate how Theorem 1 (Sec. II) works. Consider for instance the set of observables

$$\{\mathcal{O}_{1+}^b, \mathcal{O}_{2-}^b, \mathcal{O}_{1+}^c, \mathcal{O}_{1-}^c\}. \quad (18)$$

From this set of observables, one constructs the graph with boxlike topology shown in Fig. 4, which satisfies the graphical criterion posed in Theorem 1. The set (18) is composed of a selection of type B.2 taken from the shape class b and a selection of type A.1 taken from shape class c (cf. discussion in Sec. II). We now write explicitly all the possible cases for the consistency relation (15) which follow from this particular selection of observables, and thus also correspond to the graph shown in Fig. 4. Since the discrete ambiguity in case A.1 is fourfold and for B.2 it is twofold, we get the following eight relations (some multiples of 2π have already been removed

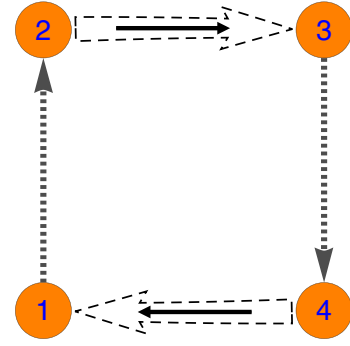


FIG. 4. The first example for a fully complete graph according to Theorem 1 from Sec. II is shown. This graph can be inferred from the selection of observables (18). The dashed single-lined arrows indicate the fact that the selection A.1 has been applied for the two observables belonging to shape class c , with corresponding relative phases $\{\phi_{12}, \phi_{34}\}$. The dashed double-lined arrows indicate the fact that a selection of type B has been applied for the two observables from the shape class b , with corresponding relative phases $\{\phi_{14}, \phi_{23}\}$. The ζ -sign arrows have been drawn into the dashed double-lined arrows, according to the selection B.2 taken from shape class b [cf. Eq. (12)].

by hand in the following equations):

$$\alpha_{12} + \zeta - \alpha_{23} + \alpha_{34} + \zeta - \alpha_{41} = 0, \quad (19)$$

$$\pi - \alpha_{12} + \zeta - \alpha_{23} + \alpha_{34} + \zeta - \alpha_{41} = 0, \quad (20)$$

$$\alpha_{12} + \zeta - \alpha_{23} + \pi - \alpha_{34} + \zeta - \alpha_{41} = 0, \quad (21)$$

$$-\alpha_{12} + \zeta - \alpha_{23} - \alpha_{34} + \zeta - \alpha_{41} = 0, \quad (22)$$

$$\alpha_{12} + \zeta + \alpha_{23} - \pi + \alpha_{34} + \zeta + \alpha_{41} - \pi = 0, \quad (23)$$

$$\pi - \alpha_{12} + \zeta + \alpha_{23} - \pi + \alpha_{34} + \zeta + \alpha_{41} - \pi = 0, \quad (24)$$

$$\alpha_{12} + \zeta + \alpha_{23} - \pi + \pi - \alpha_{34} + \zeta + \alpha_{41} - \pi = 0, \quad (25)$$

$$-\alpha_{12} + \zeta + \alpha_{23} - \pi - \alpha_{34} + \zeta + \alpha_{41} - \pi = 0. \quad (26)$$

It can be seen that no degenerate pair of equations exists in this case. This is true due to the fact that the respective transitional ζ angle ($\zeta \equiv \zeta_{1+,2-}^b$ in this case) always appears with the *same sign* in each equation. One always obtains a term “ 2ζ ” in each equation, since the ζ angles belonging to the two different relative phases ϕ_{23} and ϕ_{14} do not cancel out. The graph shown in Fig. 4 is just right for such a cancellation *not* to occur. Furthermore, we recognize the graphs constructed in Theorem 1 from Sec. II to be in principle just graphical summaries of all cases for a particular consistency relation, corresponding to a specific set of observables.

As a next example for a fully complete set, the following selection of observables is considered:

$$\{\mathcal{O}_{1+}^a, \mathcal{O}_{2-}^a, \mathcal{O}_{1+}^b, \mathcal{O}_{2+}^b\}. \quad (27)$$

This set implies the graph shown in Fig. 5. This graph satisfies all the criteria posed by Theorem 1. The observables from shape class a are picked according to the case B.2 from Sec. II, while the pair of observables from the class b has been selected according to case B.1. In both these cases, the discrete phase ambiguity is twofold. Therefore, we have to

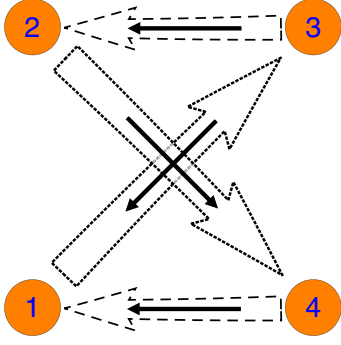


FIG. 5. The second example for a fully complete graph according to Theorem 1 from Sec. II is shown, which can be inferred from the selection of observables (27). The dashed double-lined arrows indicate a selection of type B from the shape class b (relative phases $\{\phi_{14}, \phi_{23}\}$), while the dotted double-lined arrows represent a B-type selection from shape class a (relative phases $\{\phi_{13}, \phi_{24}\}$). The ζ -sign arrows have been drawn into the respective double-lined arrows according to the selection (27).

consider the following four cases for the consistency relation (17) (again removing possible summands of 2π by hand)

$$-\zeta + \alpha_{13} + \zeta' + \alpha_{32} - \pi + \zeta - \alpha_{24} + \zeta' - \alpha_{41} = 2\zeta' + \alpha_{13} + \alpha_{32} - \alpha_{24} - \alpha_{41} - \pi = 0, \quad (28)$$

$$-\zeta + \alpha_{13} + \zeta' - \alpha_{32} + \zeta - \alpha_{24} + \zeta' + \alpha_{41} - \pi = 2\zeta' + \alpha_{13} - \alpha_{32} - \alpha_{24} + \alpha_{41} - \pi = 0, \quad (29)$$

$$-\zeta - \alpha_{13} + \pi + \zeta' + \alpha_{32} - \pi + \zeta + \alpha_{24} - \pi + \zeta' - \alpha_{41} = 2\zeta' - \alpha_{13} + \alpha_{32} + \alpha_{24} - \alpha_{41} - \pi = 0, \quad (30)$$

$$-\zeta - \alpha_{13} + \pi + \zeta' - \alpha_{32} + \zeta + \alpha_{24} - \pi + \zeta' + \alpha_{41} - \pi = 2\zeta' - \alpha_{13} - \alpha_{32} + \alpha_{24} + \alpha_{41} - \pi = 0, \quad (31)$$

where the angle $\zeta = \zeta_{1+,2-}^a$ is defined from the pair $(\mathcal{O}_{1+}^a, \mathcal{O}_{2-}^a)$, while the second angle $\zeta' \equiv \zeta_{1+,2+}^b$ belongs to the observables $(\mathcal{O}_{1+}^b, \mathcal{O}_{2+}^b)$. Again, no pair of degenerate consistency-relations exists, since the ζ' angles remain in the equations, while the ζ angles cancel each other out.

As a third example, we consider the following set:

$$\{\mathcal{O}_{1+}^b, \mathcal{O}_{2+}^b, \mathcal{O}_{1+}^c, \mathcal{O}_{2-}^c\}. \quad (32)$$

This set leads to the graph shown in Fig. 6, which does not satisfy the criteria of Theorem 1. The selection B.1 has been picked from the shape class b , while the combination B.2 has been picked from shape class c . In both cases, the discrete phase ambiguity is again twofold, which implies the following four cases for the consistency relation:

$$-\zeta + \alpha_{12} - \zeta' - \alpha_{23} + \pi + \zeta - \alpha_{34} + \zeta' - \alpha_{41} = \alpha_{12} - \alpha_{23} - \alpha_{34} - \alpha_{41} + \pi = 0, \quad (33)$$

$$-\zeta + \alpha_{12} - \zeta' + \alpha_{23} + \zeta - \alpha_{34} + \zeta' + \alpha_{41} - \pi = \alpha_{12} + \alpha_{23} - \alpha_{34} + \alpha_{41} - \pi = 0, \quad (34)$$

$$-\zeta - \alpha_{12} + \pi - \zeta' - \alpha_{23} + \pi + \zeta + \alpha_{34} - \pi + \zeta' - \alpha_{41} = -\alpha_{12} - \alpha_{23} + \alpha_{34} - \alpha_{41} + \pi = 0, \quad (35)$$

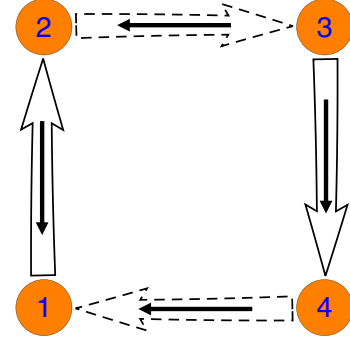


FIG. 6. The third example-graph mentioned in the main text is shown here, which can be inferred from the set of observables (32). The solid and dashed double-lined arrows have the same meaning as in Fig. 4. The ζ -sign arrows, which have been drawn inside of the double-lined arrows, correspond to the selection (32). This graph is *not* fully complete according to Theorem 1 from Sec. II.

$$-\zeta - \alpha_{12} + \pi - \zeta' + \alpha_{23} + \zeta + \alpha_{34} - \pi + \zeta' + \alpha_{41} - \pi = -\alpha_{12} + \alpha_{23} + \alpha_{34} + \alpha_{41} - \pi = 0. \quad (36)$$

The angle $\zeta = \zeta_{1+,2-}^c$ belongs here to the pair $(\mathcal{O}_{1+}^c, \mathcal{O}_{2-}^c)$, while the second angle $\zeta' \equiv \zeta_{1+,2+}^b$ is defined by the observables $(\mathcal{O}_{1+}^b, \mathcal{O}_{2+}^b)$. However, now we observe that all pairs of ζ angles cancel each other out in all the above-given equations. Then degenerate pairs of relations emerge. For instance, it is possible to transform the Eq. (34) into Eq. (35) via a multiplication by (-1) [a similar transformation relates Eqs. (33) and (36)]. Therefore, the considered set (32) is *not* fully complete.

In the same way as for the examples discussed above, we can consider all possible selections of pairs of observables, for each of the three start topologies shown in Fig. 3, then draw the graphs that follow from them and check for completeness using Theorem 1 from Sec. II. When doing this, one has 36 possible combinations for each start topology, resulting in a total of 108 combinations to consider.

We found that 60 of these 108 combinations are fully complete according to Theorem 1, using an automated procedure⁷ in Mathematica [84]. From each start topology I, II, and III, there originate 20 complete sets, respectively. The 60 complete sets found in this way are listed in the Supplemental Material [83].

In the formulation of Theorem 1 from Sec. II, as well as in the derivations discussed in this section up to this point, we always started with a given selection of observables, then drew the corresponding graph and checked this graph for

⁷Our code is really an automated way of checking the conditions of Theorem 1 algebraically, via specific checks on the orders of the indices in the respective relative phases. That is, in our code the cases for the consistency-relation are not evaluated explicitly and rather the code is doing what a person would do when checking the conditions for Theorem 1 by hand. For the photoproduction problem, one actually can check all 108 cases by hand in an acceptable timespan and thus would not need a code. This is very different for the electroproduction problem, see Sec. IV.

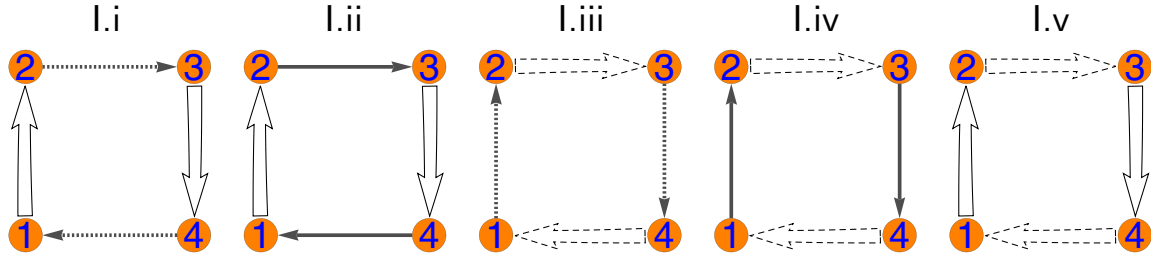


FIG. 7. These five types of graphs have been derived from the first (i.e., boxlike) topology I shown in Fig. 3. They correspond to different combinations of selections of type A and B taken from the shape classes b (relative phases $\{\phi_{14}, \phi_{23}\}$) and c (relative phases $\{\phi_{12}, \phi_{34}\}$), as described in Sec. II. At least one pair of double-lined arrows has to be contained in the graphs, i.e., at least one selection of type B has to have been made. Graphs resulting solely from selections of type A have not been shown (there exist 4 of such graphs), since they cannot yield fully complete sets (cf. Theorem 2 from Appendix A).

completeness. The reason for this is that the mapping between combinations of observables and graphs is actually *not* bijective. On other words, when starting from a specific set of observables, one can always arrive at a uniquely specified graph. However, when going in the reverse direction, i.e., when starting from a graph, one may find multiple sets of observables that fit this graph. For instance, the set of observables $\{\mathcal{O}_{1-}^b, \mathcal{O}_{2+}^b, \mathcal{O}_{1+}^c, \mathcal{O}_{1-}^c\}$ fits the graph shown in Fig. 4, exactly the same graph that originates from the first example set (18).

This leads one to question whether it is possible at all to find the above-mentioned 60 complete sets starting solely from graphs, i.e., without selecting observables first. In the following, we outline the individual steps for this alternative procedure and provide arguments for the fact that the above-mentioned nonbijectivity is actually not a problem. When deriving complete sets solely from graphs, one can proceed as follows:

- (i) Starting from one of the basic topologies with direction shown in Fig. 3, draw all possible types of graphs that result from it by applying all possible allowed combinations of pairs of single- and double-lined arrows. For the considered problem with $N = 4$ amplitudes, this would result in nine possible graph types originating from one particular start topology. However, from these nine graph types, only five contain double-lined arrows at all and thus can lead to complete sets. For the boxlike topology I, these five graph types are shown in Fig. 7.
- (ii) For each graph type obtained in (i) which contains at least one pair of double-lined arrows, draw all possible combinations of ζ -sign arrows into the given pairs of double-lined arrows. This implies 4 new graphs in case the graph type contains one pair of double-lined arrows and 16 new graphs for the one graph type shown in Fig. 7 that has two pairs of double-lined arrows. In this step one therefore obtains $(4 + 4 + 4 + 4 + 16) = 32$ graphs from each start topology. Thus, one obtains 96 graphs in total. Examples for such graphs are shown for the start topology I in Figs. 8 and 9.

- (iii) From the graphs determined in step (ii), single out all graphs that satisfy the completeness criterion posed in Theorem 1. For each graph type containing one pair of double-lined arrows shown in Fig. 7, one obtains two complete cases of combinations of ζ signs, cf. Fig. 8. For each graph type that has two pairs of double-lined arrows as shown in Fig. 7, one gets 12 complete combinations of ζ signs, see Fig. 9. Thus, one obtains $(2 + 2 + 2 + 2 + 12) = 20$ fully complete graphs from each start topology and therefore 60 fully complete graphs in total. We observe that the combinatorics match with the case discussed before, where we started from selections of observables.
- (iv) For each complete graph obtained in step (iii), find all selections of observables that fit it according to the cases A.1, A.2, and B.1–B.4 listed in Sec. II. Here, one runs into the problem that the graphs constructed in steps (i)–(iii) allow for more combinations of ζ signs than exist in the cases listed in Sec. II. In the cases B.1–B.4 from Sec. II, the possible combinations of the signs of the ζ 's in the ambiguity formulas for

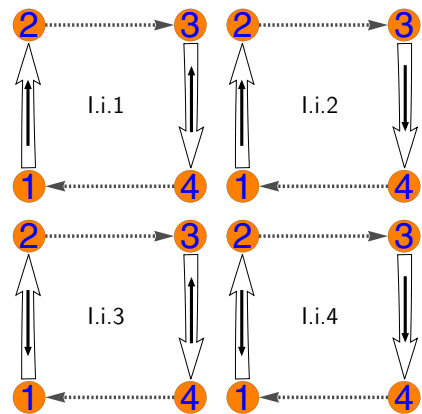


FIG. 8. These four graphs are directly deduced from graph type (I.i) shown in Fig. 7, by inserting all possible combinations of ζ -sign arrows into the double-lined arrows. The two graphs (I.i.2) and (I.i.3) satisfy all the completeness conditions posed by Theorem 1 from Sec. II, while the graphs (I.i.1) and (I.i.4) violate these criteria.

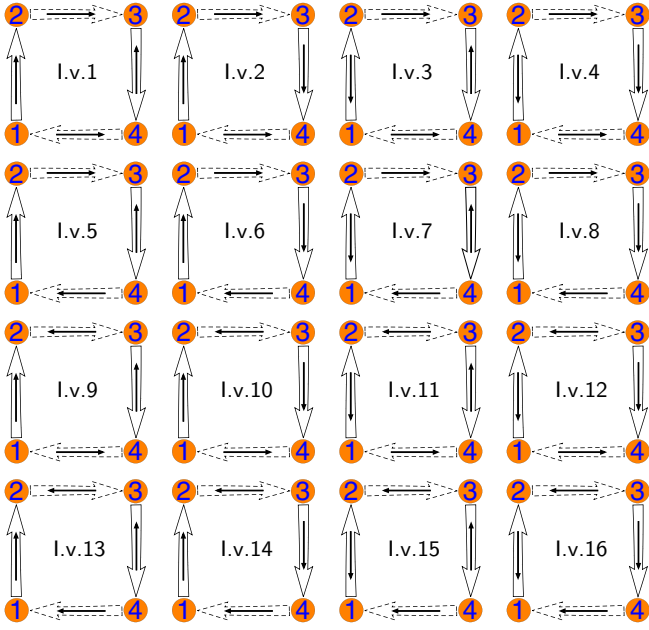


FIG. 9. This set of 16 graphs is directly deduced from graph type (I.v) shown in Fig. 7, by inserting all possible combinations of ζ -sign arrows into the double-lined arrows. From these 16 graphs, only four violate the completeness criterion posed in Theorem 1 of Sec. II, namely: (I.v.1), (I.v.4), (I.v.13), and (I.v.16).

(ϕ_{ij}, ϕ_{kl}) were $(-\zeta, -\zeta)$ and $(-\zeta, +\zeta)$. This leads one to question to which combinations of observables the other two cases for the ζ signs, i.e., $(+\zeta, +\zeta)$ and $(+\zeta, -\zeta)$, correspond.

As described in detail in Appendix C and summarized in Table II, the “new” cases $(+\zeta, +\zeta)$ and $(+\zeta, -\zeta)$ just correspond to the already known pairings of observables listed in Sec. II, but with the sign of one of the two observables flipped. Therefore, these new cases introduce in principle redundant information, but they still can be very useful for the derivation of complete sets when starting solely from graphs.

As an example, consider the two complete graphs (I.i.2) and (I.i.3) shown in Fig. 8. These graphs are related to each by a flip of the direction of both ζ -

sign arrows within the appearing pair of double-lined arrows. These two graphs correspond to the same observables: The graph (I.i.3) corresponds to the sets

$$\{\mathcal{O}_{1+}^b, \mathcal{O}_{1-}^b, \mathcal{O}_{1+}^c, \mathcal{O}_{2+}^c\} \quad \text{and} \\ \{\mathcal{O}_{1+}^b, \mathcal{O}_{1-}^b, \mathcal{O}_{1-}^c, \mathcal{O}_{2-}^c\}, \quad (37)$$

while the graph (I.i.2) corresponds to the sets (cf. Table II)

$$\{\mathcal{O}_{1+}^b, \mathcal{O}_{1-}^b, \mathcal{O}_{1+}^c, -\mathcal{O}_{2+}^c\} \quad \text{and} \\ \{\mathcal{O}_{1+}^b, \mathcal{O}_{1-}^b, \mathcal{O}_{1-}^c, -\mathcal{O}_{2-}^c\}. \quad (38)$$

In this way, we see that graphs related to each other by the flip of *one* pair of ζ -sign arrows generally introduce redundant information. However, this does not harm our ability to derive all 60 complete sets starting solely from graphs, since during the steps (i) to (iii) outlined above, we have determined all possible fully complete graphs anyway. We just have to assign all complete sets of observables to each graph that is fully complete according to Theorem 1, using the associations shown in Table II. Then, from the resulting overall sets of observables, we have to sort out the nonredundant ones, which should then leave only the 60 complete sets which we already determined when starting from the 108 possible combinations of observables.

The steps (i)–(iv) described above can in principle be automated on a computer.

We report that all relevant complete sets found by Nakayama in the case (2+2) (cf. [73]) have been recovered using the graphical criterion devised in Theorem 1 from Sec. II. Furthermore, we also verified the completeness of the obtained sets with Mathematica [84], using similar methods as those described in Appendix A of Ref. [76]. We refrain from listing all these complete sets here again, due to reasons of space. The sets have been collected in the Supplemental Material [83]. The photoproduction problem has already been treated at length in the literature. Therefore, we refer to tables and lists already given in Refs. [52,73] for a further confirmation of our results.

TABLE II. The different cases for the signs of the ζ angles are given here, as they appear in the formulas for the discrete ambiguities for the relative phases ϕ_{ij} and ϕ_{kl} , as listed in Sec. II. The possible selections of pairs of observables (including possible sign flips for both observables), which correspond to the different sign combinations for the ζ 's, are given on the right. The cases $(-\zeta, -\zeta)$ and $(-\zeta, +\zeta)$ have been listed in Sec. II and derived explicitly in Appendix B. The other two cases $(+\zeta, -\zeta)$ and $(+\zeta, +\zeta)$ follow from flipping the sign of one of the two observables in the respective pairs and thus give in principle redundant information. However, the information given in this table is still useful in case one wishes to derive complete sets of observables starting solely from graphs, as described in the main text. Further details on how the results shown here were obtained are given in Appendix C.

$(\zeta \text{ sign for } \phi_{ij}, \zeta \text{ sign for } \phi_{kl})$	Possible selections of observables
$(-\zeta, -\zeta)$	$(\mathcal{O}_{1+}^n, \mathcal{O}_{2+}^n), (-\mathcal{O}_{1+}^n, -\mathcal{O}_{2+}^n), (\mathcal{O}_{1-}^n, \mathcal{O}_{2-}^n), (-\mathcal{O}_{1-}^n, -\mathcal{O}_{2-}^n)$
$(-\zeta, +\zeta)$	$(\mathcal{O}_{1+}^n, \mathcal{O}_{2-}^n), (-\mathcal{O}_{1+}^n, -\mathcal{O}_{2-}^n), (\mathcal{O}_{1-}^n, \mathcal{O}_{2+}^n), (-\mathcal{O}_{1-}^n, -\mathcal{O}_{2+}^n)$
$(+\zeta, -\zeta)$	$(-\mathcal{O}_{1+}^n, \mathcal{O}_{2-}^n), (\mathcal{O}_{1+}^n, -\mathcal{O}_{2-}^n), (-\mathcal{O}_{1-}^n, \mathcal{O}_{2+}^n), (\mathcal{O}_{1-}^n, -\mathcal{O}_{2+}^n)$
$(+\zeta, +\zeta)$	$(-\mathcal{O}_{1+}^n, \mathcal{O}_{2+}^n), (\mathcal{O}_{1+}^n, -\mathcal{O}_{2+}^n), (-\mathcal{O}_{1-}^n, \mathcal{O}_{2-}^n), (\mathcal{O}_{1-}^n, -\mathcal{O}_{2-}^n)$

It should come as no surprise that the results obtained by Nakayama were reproduced by Theorem 1 from Sec. II, since this theorem is basically a graphical reformulation of derivations and criteria already contained in Ref. [73] (see in particular Sec. III there). However, the usefulness of the proposed graphical criterion will become apparent once we utilize it in order to derive complete sets of minimal length for the more involved problem of single-meson electroproduction, which will be the subject of the next section.

IV. APPLICATION TO PSEUDOSCALAR MESON ELECTROPRODUCTION ($N = 6$)

Pseudoscalar meson electroproduction is described by $N = 6$ amplitudes b_1, \dots, b_6 , which are accompanied by 36 polarization observables [74]. The expressions for the observables are collected in Table III. Again, an algebra of Dirac matrices is behind the definitions of the observables and therefore also behind their subdivision into different shape classes [69]. This time, one has the 6×6 Dirac matrices $\tilde{\Gamma}^\alpha$ (these are listed in Appendix B of Ref. [69]). For the observables in non-diagonal shape classes, we again use the systematic notation $\mathcal{O}_{v\pm}^n$ introduced by Nakayama [73]. However, in Table III, we also give the observables in the usual physical notation, which is taken from the paper by Tiator and collaborators [74] and which states that each observable corresponds to a so-called response function $R_i^{\beta\alpha}$. The (physical) meaning of the indices on these response-functions is explained further in Table III.

The observables (and thus also the corresponding $\tilde{\Gamma}^\alpha$ matrices) can be grouped into 10 overall shape classes. Two shape classes contain diagonal observables: one of these two classes, called D1, contains 4 observables which correspond to matrices with nonvanishing entries in the first four diagonal elements. The second diagonal shape class D2 contains 2 matrices with nonvanishing entries in the fifth and sixth diagonal element. The remaining 30 observables are divided into 8 nondiagonal shape classes. These nondiagonal classes comprise four shape classes of antidiagonal structure (AD1–AD4), three shape classes of right-parallel-gram type (PR1–PR3) and one class of left-parallel-gram structure (PL1). All nondiagonal shape classes each contain 4 observables, apart from the class AD2 which is composed of just two quantities.

We again make the standard assumption that all six observables $\{R_T^{00}, {}^cR_{TT}^{00}, R_T^{0y}, R_T^{y0}, R_L^{00}, R_L^{0y}\}$ from the diagonal shape classes D1 and D2 have been already used to uniquely fix the six moduli $|b_1|, \dots, |b_6|$. Then, one has to select six more observables from the remaining nondiagonal shape classes, which corresponds to the determination of complete sets with minimal length $2N = 12$. Such minimal complete sets should then be able to uniquely specify the relative phases. This is where we again use the criterion formulated in Theorem 1 of Sec. II.

For the problem of electroproduction ($N = 6$ amplitudes), there exist 60 possible topologies for fully connected graphs with 6 vertices, where every vertex has order 2 (i.e., is touched by two edges). We refrain here from showing all these 60 topologies, due to reasons of space. They can be found in Sec. VI of Ref. [69]. The additional constraints formulated

for the considered graphs in the beginning of Theorem 1 from Sec. II place further restrictions on the topologies. We have only to consider those topologies which correspond to three pairs of relative phases from three different shape classes of four (cf. Table III). From the above-mentioned total of 60 possible topologies, only 8 topologies remain that satisfy this constraint. These 8 possibilities are shown in Fig. 10. They constitute the possible start topologies for our application of Theorem 1 to electroproduction.

Each of the eight start topologies corresponds to a particular combination of observables from three different shape classes. Furthermore, the directions for the graphs shown in Fig. 10 stand in a one-to-one correspondence to our convention for writing the consistency relations (cf. the comments made below Eq. (5) in Sec. II). The consistency relations corresponding to the 8 topologies shown in Fig. 10 read as follows:

$$\begin{aligned} \text{I} = (a, e, g): \phi_{13} + \phi_{36} + \phi_{62} + \phi_{24} + \phi_{45} + \phi_{51} \\ = 0, \end{aligned} \quad (39)$$

$$\begin{aligned} \text{II} = (a, f, h): \phi_{13} + \phi_{35} + \phi_{52} + \phi_{24} + \phi_{46} + \phi_{61} \\ = 0, \end{aligned} \quad (40)$$

$$\begin{aligned} \text{III} = (b, e, f): \phi_{14} + \phi_{45} + \phi_{52} + \phi_{23} + \phi_{36} + \phi_{61} \\ = 0, \end{aligned} \quad (41)$$

$$\begin{aligned} \text{IV} = (b, g, h): \phi_{14} + \phi_{46} + \phi_{62} + \phi_{23} + \phi_{35} + \phi_{51} \\ = 0, \end{aligned} \quad (42)$$

$$\begin{aligned} \text{V} = (c, e, f): \phi_{12} + \phi_{25} + \phi_{54} + \phi_{43} + \phi_{36} + \phi_{61} \\ = 0, \end{aligned} \quad (43)$$

$$\begin{aligned} \text{VI} = (c, e, g): \phi_{12} + \phi_{26} + \phi_{63} + \phi_{34} + \phi_{45} + \phi_{51} \\ = 0, \end{aligned} \quad (44)$$

$$\begin{aligned} \text{VII} = (c, f, h): \phi_{12} + \phi_{25} + \phi_{53} + \phi_{34} + \phi_{46} + \phi_{61} \\ = 0, \end{aligned} \quad (45)$$

$$\begin{aligned} \text{VIII} = (c, g, h): \phi_{12} + \phi_{26} + \phi_{64} + \phi_{43} + \phi_{35} + \phi_{51} \\ = 0. \end{aligned} \quad (46)$$

We stress again the fact that the sign conventions fixed by these directions are of vital importance for the applicability of Theorem 1.

As a first example for a selection of six observables from the nondiagonal shape classes (i.e., of three pairs of observables), we consider the following set:

$$\{\mathcal{O}_{1+}^a, \mathcal{O}_{2+}^a, \mathcal{O}_{1+}^e, \mathcal{O}_{1-}^e, \mathcal{O}_{2+}^g, \mathcal{O}_{2-}^g\}, \quad (47)$$

which implies the graph shown in Fig. 11. This specific graph fulfills the completeness criterion posed in Theorem 1 and therefore the set (47) is in fact complete. When combined with the six observables from the diagonal shape classes D1 and D2, the set (47) thus forms a complete set of minimal length $2N = 12$. We refrain here from writing all the cases for the consistency relation (39) explicitly and instead again mention the fact that the graph shown in Fig. 11 constitutes a useful summary of all these cases.

TABLE III. The definitions of electroproduction observables are collected here for the diagonal observables of types D1 and D2, as well as for the nondiagonal shape classes $\{a, b, c, d, e, f, g, h\}$. The specific combinations of relative phases belonging to each individual nondiagonal shape class are indicated as well. The definitions and sign conventions for the observables have been adopted from Ref. [74]. Every observable from a nondiagonal shape class is written in the systematic symbolic notation $\mathcal{O}_{v\pm}^n$ introduced by Nakayama [73]. Furthermore, we also give for the observables the usual physical notation, which is defined as follows [74]: Every observable corresponds to a “response function,” $R_i^{\beta\alpha}$. The superscript index α represents the target polarization, the index β indicates the recoil polarization and the subscript i represents the polarization of the virtual photon in electroproduction, which can take the following configurations: $i \in \{T, L, TL, TT, TL', TT'\}$ (meaning purely longitudinal, purely transverse or “mixed” interference contributions to the differential cross section). In case the letter “s” or “c” is written as an additional superscript on the left of the respective response function, then this indicates a possible sine or cosine dependence of the respective contribution to the differential cross section (with the sine or cosine depending on the azimuthal angle of the produced pseudoscalar meson).

Observable	Relative phases	Shape class
$R_T^{00} = \frac{1}{2}(b_1 ^2 + b_2 ^2 + b_3 ^2 + b_4 ^2)$		D1
$-{}^c R_{TT}^{00} = \frac{1}{2}(b_1 ^2 + b_2 ^2 - b_3 ^2 - b_4 ^2)$		
$-R_T^{0y} = \frac{1}{2}(- b_1 ^2 + b_2 ^2 + b_3 ^2 - b_4 ^2)$		
$-R_T^{y0} = \frac{1}{2}(- b_1 ^2 + b_2 ^2 - b_3 ^2 + b_4 ^2)$		
$\mathcal{O}_{1+}^a = b_1 b_3 \sin \phi_{13} + b_2 b_4 \sin \phi_{24} = \text{Im}[b_3^* b_1 + b_4^* b_2] = -{}^s R_{TT}^{0z}$	$\{\phi_{13}, \phi_{24}\}$	$a = \text{PR1}$
$\mathcal{O}_{1-}^a = b_1 b_3 \sin \phi_{13} - b_2 b_4 \sin \phi_{24} = \text{Im}[b_3^* b_1 - b_4^* b_2] = R_{TT'}^{0x}$		
$\mathcal{O}_{2+}^a = b_1 b_3 \cos \phi_{13} + b_2 b_4 \cos \phi_{24} = \text{Re}[b_3^* b_1 + b_4^* b_2] = R_{TT'}^{0z}$		
$\mathcal{O}_{2-}^a = b_1 b_3 \cos \phi_{13} - b_2 b_4 \cos \phi_{24} = \text{Re}[b_3^* b_1 - b_4^* b_2] = {}^s R_{TT'}^{0x}$		
$\mathcal{O}_{1+}^b = b_1 b_4 \sin \phi_{14} + b_2 b_3 \sin \phi_{23} = \text{Im}[b_4^* b_1 + b_3^* b_2] = -{}^s R_{TT'}^{z0}$	$\{\phi_{14}, \phi_{23}\}$	$b = \text{AD1}$
$\mathcal{O}_{1-}^b = b_1 b_4 \sin \phi_{14} - b_2 b_3 \sin \phi_{23} = \text{Im}[b_4^* b_1 - b_3^* b_2] = -R_{TT'}^{x0}$		
$\mathcal{O}_{2+}^b = b_1 b_4 \cos \phi_{14} + b_2 b_3 \cos \phi_{23} = \text{Re}[b_4^* b_1 + b_3^* b_2] = R_{TT'}^{z0}$		
$\mathcal{O}_{2-}^b = b_1 b_4 \cos \phi_{14} - b_2 b_3 \cos \phi_{23} = \text{Re}[b_4^* b_1 - b_3^* b_2] = -{}^s R_{TT'}^{x0}$		
$\mathcal{O}_{1+}^c = b_1 b_2 \sin \phi_{12} + b_3 b_4 \sin \phi_{34} = \text{Im}[b_2^* b_1 + b_4^* b_3] = -R_T^{xz}$	$\{\phi_{12}, \phi_{34}\}$	$c = \text{PL1}$
$\mathcal{O}_{1-}^c = b_1 b_2 \sin \phi_{12} - b_3 b_4 \sin \phi_{34} = \text{Im}[b_2^* b_1 - b_4^* b_3] = R_T^{zx}$		
$\mathcal{O}_{2+}^c = b_1 b_2 \cos \phi_{12} + b_3 b_4 \cos \phi_{34} = \text{Re}[b_2^* b_1 + b_4^* b_3] = R_T^{z\bar{z}}$		
$\mathcal{O}_{2-}^c = b_1 b_2 \cos \phi_{12} - b_3 b_4 \cos \phi_{34} = \text{Re}[b_2^* b_1 - b_4^* b_3] = R_T^{x\bar{x}}$		
$R_L^{00} = b_5 ^2 + b_6 ^2$		D2
$R_L^{0y} = b_5 ^2 - b_6 ^2$		
$\mathcal{O}_1^d = 2 b_5 b_6 \sin \phi_{56} = 2\text{Im}[b_6^* b_5] = R_L^{z\bar{x}}$	$\{\phi_{56}\}$	$d = \text{AD2}$
$\mathcal{O}_2^d = 2 b_5 b_6 \cos \phi_{56} = 2\text{Re}[b_6^* b_5] = -R_L^{x\bar{z}}$		
$\mathcal{O}_{1+}^e = b_3 b_6 \sin \phi_{36} + b_4 b_5 \sin \phi_{45} = \text{Im}[b_6^* b_3 + b_5^* b_4] = -{}^s R_{LT'}^{00}$	$\{\phi_{36}, \phi_{45}\}$	$e = \text{AD3}$
$\mathcal{O}_{1-}^e = b_3 b_6 \sin \phi_{36} - b_4 b_5 \sin \phi_{45} = \text{Im}[b_6^* b_3 - b_5^* b_4] = {}^s R_{LT'}^{0y}$		
$\mathcal{O}_{2+}^e = b_3 b_6 \cos \phi_{36} + b_4 b_5 \cos \phi_{45} = \text{Re}[b_6^* b_3 + b_5^* b_4] = {}^c R_{LT}^{00}$		
$\mathcal{O}_{2-}^e = b_3 b_6 \cos \phi_{36} - b_4 b_5 \cos \phi_{45} = \text{Re}[b_6^* b_3 - b_5^* b_4] = -{}^c R_{LT}^{0y}$		
$\mathcal{O}_{1+}^f = b_1 b_6 \sin \phi_{16} + b_2 b_5 \sin \phi_{25} = \text{Im}[b_6^* b_1 + b_5^* b_2] = -{}^s R_{LT}^{0z}$	$\{\phi_{16}, \phi_{25}\}$	$f = \text{AD4}$
$\mathcal{O}_{1-}^f = b_1 b_6 \sin \phi_{16} - b_2 b_5 \sin \phi_{25} = \text{Im}[b_6^* b_1 - b_5^* b_2] = {}^c R_{LT'}^{0x}$		
$\mathcal{O}_{2+}^f = b_1 b_6 \cos \phi_{16} + b_2 b_5 \cos \phi_{25} = \text{Re}[b_6^* b_1 + b_5^* b_2] = {}^c R_{LT'}^{0z}$		
$\mathcal{O}_{2-}^f = b_1 b_6 \cos \phi_{16} - b_2 b_5 \cos \phi_{25} = \text{Re}[b_6^* b_1 - b_5^* b_2] = {}^s R_{LT}^{0x}$		
$\mathcal{O}_{1+}^g = b_1 b_5 \sin \phi_{15} + b_2 b_6 \sin \phi_{26} = \text{Im}[b_5^* b_1 + b_6^* b_2] = -{}^s R_{LT}^{z0}$	$\{\phi_{15}, \phi_{26}\}$	$g = \text{PR2}$
$\mathcal{O}_{1-}^g = b_1 b_5 \sin \phi_{15} - b_2 b_6 \sin \phi_{26} = \text{Im}[b_5^* b_1 - b_6^* b_2] = -{}^c R_{LT'}^{x0}$		
$\mathcal{O}_{2+}^g = b_1 b_5 \cos \phi_{15} + b_2 b_6 \cos \phi_{26} = \text{Re}[b_5^* b_1 + b_6^* b_2] = {}^c R_{LT'}^{z0}$		
$\mathcal{O}_{2-}^g = b_1 b_5 \cos \phi_{15} - b_2 b_6 \cos \phi_{26} = \text{Re}[b_5^* b_1 - b_6^* b_2] = -{}^s R_{LT'}^{x0}$		
$\mathcal{O}_{1+}^h = b_3 b_5 \sin \phi_{35} + b_4 b_6 \sin \phi_{46} = \text{Im}[b_5^* b_3 + b_6^* b_4] = {}^s R_{LT'}^{zx}$	$\{\phi_{35}, \phi_{46}\}$	$h = \text{PR3}$
$\mathcal{O}_{1-}^h = b_3 b_5 \sin \phi_{35} - b_4 b_6 \sin \phi_{46} = \text{Im}[b_5^* b_3 - b_6^* b_4] = -{}^c R_{LT'}^{z\bar{x}}$		
$\mathcal{O}_{2+}^h = b_3 b_5 \cos \phi_{35} + b_4 b_6 \cos \phi_{46} = \text{Re}[b_5^* b_3 + b_6^* b_4] = -{}^c R_{LT}^{x\bar{z}}$		
$\mathcal{O}_{2-}^h = b_3 b_5 \cos \phi_{35} - b_4 b_6 \cos \phi_{46} = \text{Re}[b_5^* b_3 - b_6^* b_4] = -{}^s R_{LT}^{z\bar{x}}$		

As a second example set, we consider the following selection of six observables

$$\{\mathcal{O}_{1+}^a, \mathcal{O}_{2-}^a, \mathcal{O}_{1-}^e, \mathcal{O}_{2+}^e, \mathcal{O}_{2+}^g, \mathcal{O}_{2-}^g\}, \quad (48)$$

which implies the graph shown in Fig. 12. This graph violates the completeness criterion from Theorem 1 and therefore the set (48) is not complete.

The search for all complete sets using Theorem 1 can again proceed via considerations of all relevant combinations of observables (cf. the discussion in Sec. III). For each of the 8 possible start topologies shown in Fig. 10, one then has to consider 216 combinations, which are made up of all the possibilities to select three pairs of observables using the cases A.1–B.4 outlined in Sec. II. Thus, there exists a total of $(8 * 216) = 1728$ combinations that have to be

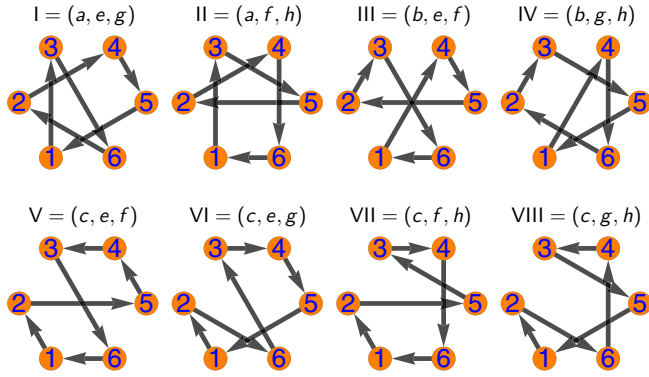


FIG. 10. The 8 possible start topologies for pseudoscalar meson electroproduction ($N = 6$ amplitudes), which allow for a selection of three pairs of observables from three different shape classes, are shown here. The *direction of translation* is indicated for each graph as well. This direction is intimately connected to our convention of writing the corresponding consistency relation, i.e., Eqs. (39) to (46) (see also the comments made below Eq. (5) in Sec. II). Each of the shown topologies corresponds to the relative phases from a particular combination of three shape classes for electroproduction (cf. Table III). The combinations of shape classes are also indicated above the graphs (cf. discussion in the main text).

considered. Using the Mathematica routines already mentioned in Sec. III, we found 1216 combinations from these 1728 different possibilities to be fully complete. These complete sets are composed of 152 sets for each of the 8 start topologies shown in Fig. 10. One example set for each start topology is given in Table IV. The full list of 1216 complete sets is given in the Supplemental Material [83].

Conversely, one can also derive the 1216 complete sets starting solely from considerations of graphs, similar to the steps (i) to (iv) described at the end of Sec. III. From each of the 8 start topologies shown in Fig. 10, one can derive 19 different types of graphs that contain at least one pair of double-lined arrows. These 19 graph types are plotted for the first start topology ‘I’ in Fig. 13. Then, one has to draw

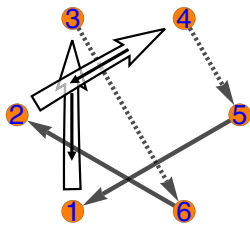


FIG. 11. The first example for a graph in electroproduction ($N = 6$ amplitudes) is shown. This graph is fully complete according to Theorem 1 from Sec. II. It can be inferred from the selection of observables (47). The dashed single-lined arrows indicate the selection of type A.1 for the shape class e , while the solid single-lined arrows represent the selection of type A.2 for the shape class g . The solid double-lined arrows indicate the fact that a selection of type B has been applied for the two observables from the shape class a . The ζ -sign arrows have been drawn into the solid double-lined arrows according to the selection (47).

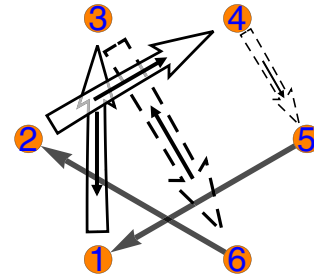


FIG. 12. The second example graph for electroproduction is shown. This graph violates the completeness criterion posed in Theorem 1 from Sec. II. It can be inferred from the selection of observables (48). The solid single-lined arrows indicate the selection of type A.2 for the shape class g . The solid double-lined arrows indicate the fact that a selection of type B has been applied for the two observables from the shape class a , while the dashed double-lined arrows represent the same fact for the relative phases belonging to shape class e . The ζ -sign arrows have been drawn into the double-lined arrows according to the selection (48).

all possible combinations of ζ -sign arrows into the double-lined arrows in the relevant graph types. For each graph type with one pair of double-lined arrows, one thus obtains 4 graphs with ζ -sign arrows, each graph type with two pairs of double-lined arrows implies 16 graphs with ζ -sign arrows and for the one possible graph type (one per start topology) which contains three pairs of double-lined arrows, one gets 64 possible graphs with ζ -sign arrows. Therefore, for each start topology, $(12 * 4 + 6 * 16 + 1 * 64) = 208$ graphs have to be considered (cf. Fig. 13). From these 208 graphs, 152 turn out to fulfill the completeness criteria⁸ posed in Theorem 1 from Sec. II. For all start topologies, this leads to $(8 * 152) = 1216$ complete graphs. Again, the combinatorics in the purely graphical approach match exactly the number of complete sets which has been determined by starting from all possible combinations of observables, i.e., in the first approach outlined above.

In the following, we discuss the general structure of the 1216 derived complete sets in a bit more detail and also compare them to complete sets for electroproduction already discussed in the literature [69,74]. Due to the basic structure of the 8 start topologies shown in Fig. 10, one always obtains a combination of two observables from one of the shape classes with purely transverse photon polarization $\{a, b, c\}$ with four observables from two of the shape classes with mixed transverse-longitudinal photon polarization $\{e, f, g, h\}$ (cf. also Table IV). These observables of course always have to be combined with the six “diagonal” observables

⁸In more details: Each graph type with one pair of double-lined arrows implies 2 complete graphs, each graph type with two pairs of double-lined arrows implies 12 complete graphs, and the one graph type (one per start topology) with three pairs of double-lined arrows implies 56 complete graphs. Thus, one gets $(12 * 2 + 6 * 12 + 1 * 56) = 152$ complete graphs from each of the 8 possible start topologies (see also Fig. 13).

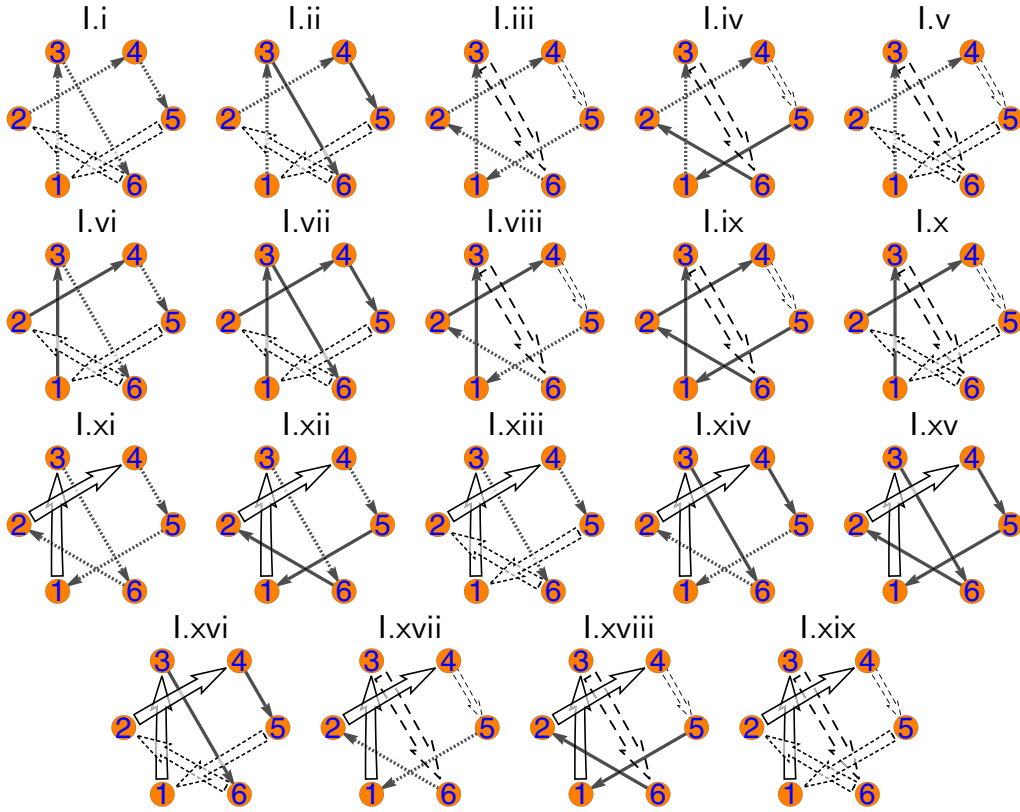


FIG. 13. These nineteen types of graphs arise from the first topology with direction shown in Fig. 10. They correspond to different combinations of selections of types A and B (cf. Sec. II) for the three pairs of relative phases belonging to the shape classes (a, e, g) (i.e., pairs of relative phases $\{\phi_{13}, \phi_{24}\}$, $\{\phi_{36}, \phi_{45}\}$ and $\{\phi_{15}, \phi_{26}\}$, respectively), with at least one pair of double-lined arrows, i.e., at least one selection of type B. The solid double-lined arrows mark relative phases belonging to the shape class a , dashed double-lined arrows mark relative phases from the shape class e and the dotted double-lined arrows refer to the shape class g . Graphs resulting solely from selections of type A are not shown in this plot (there exist eight such graphs), since they cannot yield fully complete sets according to Theorem 2 from Appendix A.

$\{R_T^{00}, {}^c R_{TT}^{00}, R_T^{0y}, R_T^{y0}, R_L^{00}, R_L^{0y}\}$, where the latter six quantities are composed of both purely transverse and purely longitudinal observables. Furthermore, for each of the 8 shape combinations corresponding to one of the 8 start topologies shown in Fig. 10, there always occurs at least one shape class that contains only observables with recoil polarization, i.e., one of the shape classes $\{b, c, g, h\}$. This means that just as in the case of photoproduction [52,73], double-polarization observables with recoil polarization cannot be avoided for a minimal complete set in electroproduction, at least within the context of the search strategy employed in the present work. This fact has also been pointed out in the work on electroproduction by Tiator and collaborators [74]. Furthermore, the unavoidability of double-polarization observables with recoil polarization has also turned out to be true for the Moravcsik-complete sets⁹ consisting of 13 as well as 14 observables, which have been derived and listed for electroproduction in Ref. [69].

Another interesting property of the minimal complete sets given for electroproduction in Table IV as well as the supplemental material [83] is that they contain no observables from the purely longitudinal shape class AD2, i.e., none of the observables $\{R_L^{zx}, R_L^{yx}\}$. This fact is a consequence of the shapes of the 8 start topologies, since the relative phase ϕ_{56} is never present in any of them. This is very different from the Moravcsik-complete sets with 13 observables derived in Ref. [69], since one observable from the pair $\{R_L^{zx}, R_L^{yx}\}$ is contained in all of them.

Furthermore, it is interesting to analyze the 1216 minimal complete sets regarding their recoil-polarization content. For each of the shape class combinations (a, e, g) , (a, f, h) , (b, e, f) , and (c, e, f) , or equivalently for each of the four corresponding start topologies (cf. Fig. 10), one obtains a complete set that contains exactly two recoil-polarization observables, apart from the observable R_T^{y0} which is contained in the six “diagonal” observables and thus always measured, of course. For each of the two shape class combinations (c, e, g) and (c, f, h) , one gets a complete set with four recoil-polarization observables (apart from R_T^{y0}) and for each of the combinations (b, g, h) and (c, g, h) , one gets a complete set with the maximal recoil-polarization content of six

⁹We denote complete sets of observables derived using Theorem 2 from Appendix A as “Moravcsik-complete sets,” cf. Ref. [69].

TABLE IV. Here we collect 8 selected examples for the minimal complete sets composed of 12 observables. One example has been chosen for each of the 8 different start topologies shown in Fig. 10. The 6 observables given here in each case have to be combined with the 6 diagonal observables $\{R_T^{00}, {}^cR_{TT}^{00}, R_T^{0y}, R_T^{y0}, R_L^{00}, R_L^{0y}\}$ in order to form a complete set of 12. Every example is given in the response function notation $R_i^{\beta\alpha}$ and also in Nakayama's [73] systematic notation $\mathcal{O}_{i\pm}^n$ (cf. Table III). The labeling scheme for the set number contains the combination of shape classes for each of the 8 start topologies, as well as the number that the respective set has been given in the full lists contained in the Supplemental Material [83]. This Table contains the first example set (47) (i.e., the graph shown in Fig. 11) discussed in the main text, which is here the example for the shape class combination “(a, e, g).” The Supplemental Material [83] contains all 1216 minimal complete sets derived for electroproduction in this work. These 1216 minimal complete sets can be further subdivided into 152 complete sets for each of the 8 relevant shape-class combinations, i.e., for each of the 8 relevant start topologies.

Set number	Observables					
(a, e, g) : 42	${}^sR_{TT}^{0z}$	$R_{TT'}^{0z}$	${}^sR_{LT'}^{00}$	${}^sR_{LT'}^{0y}$	${}^cR_{LT'}^{z0}$	${}^sR_{LT'}^{x0}$
	\mathcal{O}_{1+}^a	\mathcal{O}_{2+}^a	\mathcal{O}_{1+}^e	\mathcal{O}_{1-}^e	\mathcal{O}_{2+}^g	\mathcal{O}_{2-}^g
(a, f, h) : 10	${}^sR_{TT}^{0z}$	$R_{TT'}^{0x}$	${}^sR_{LT'}^{0z}$	${}^cR_{LT'}^{0z}$	${}^cR_{LT'}^{zx}$	${}^sR_{LT'}^{zx}$
	\mathcal{O}_{1+}^a	\mathcal{O}_{1-}^a	\mathcal{O}_{1+}^f	\mathcal{O}_{2+}^f	\mathcal{O}_{1-}^h	\mathcal{O}_{2-}^h
(b, e, f) : 100	$R_{TT'}^{x0}$	$R_{TT'}^{z0}$	${}^cR_{LT}^{00}$	${}^cR_{LT}^{0y}$	${}^cR_{LT}^{0x}$	${}^sR_{LT}^{0x}$
	\mathcal{O}_{1-}^b	\mathcal{O}_{2+}^b	\mathcal{O}_{2+}^e	\mathcal{O}_{2-}^e	\mathcal{O}_{1-}^f	\mathcal{O}_{2-}^f
(b, g, h) : 150	$R_{TT'}^{x0}$	${}^sR_{TT}^{x0}$	${}^cR_{LT}^{x0}$	${}^sR_{LT}^{x0}$	${}^sR_{LT}^{xx}$	${}^sR_{LT}^{zx}$
	\mathcal{O}_{1-}^b	\mathcal{O}_{2-}^b	\mathcal{O}_{1-}^g	\mathcal{O}_{2-}^g	\mathcal{O}_{1+}^h	\mathcal{O}_{2-}^h
(c, e, f) : 30	R_T^{z0}	R_T^{zx}	${}^sR_{LT'}^{00}$	${}^cR_{LT'}^{0y}$	${}^sR_{LT'}^{0z}$	${}^sR_{LT'}^{0x}$
	\mathcal{O}_{2+}^c	\mathcal{O}_{2-}^c	\mathcal{O}_{1+}^e	\mathcal{O}_{2-}^e	\mathcal{O}_{1+}^f	\mathcal{O}_{2-}^f
(c, e, g) : 80	R_T^{zx}	R_T^{xx}	${}^cR_{LT}^{00}$	${}^cR_{LT}^{0y}$	${}^cR_{LT}^{x0}$	${}^cR_{LT}^{z0}$
	\mathcal{O}_{1+}^c	\mathcal{O}_{2-}^c	\mathcal{O}_{2+}^e	\mathcal{O}_{2-}^e	\mathcal{O}_{1-}^g	\mathcal{O}_{2+}^g
(c, f, h) : 1	R_T^{zx}	R_T^{zx}	${}^sR_{LT}^{0z}$	${}^cR_{LT}^{0x}$	${}^sR_{LT}^{xx}$	${}^sR_{LT}^{zx}$
	\mathcal{O}_{1+}^c	\mathcal{O}_{1-}^c	\mathcal{O}_{1+}^f	\mathcal{O}_{1-}^f	\mathcal{O}_{1+}^h	\mathcal{O}_{2-}^h
(c, g, h) : 50	R_T^{z0}	R_T^{z0}	${}^sR_{LT}^{x0}$	${}^sR_{LT}^{x0}$	${}^sR_{LT}^{xx}$	${}^sR_{LT}^{zx}$
	\mathcal{O}_{1+}^c	\mathcal{O}_{2+}^c	\mathcal{O}_{1+}^g	\mathcal{O}_{2-}^g	\mathcal{O}_{1+}^h	\mathcal{O}_{2-}^h

recoil-polarization observables. The statements made here are reflected in the 8 example sets shown in Table IV.

Further interesting facts arise as soon as we compare the 1216 minimal complete sets derived in this work to the 96 possible Moravcsik-complete sets composed of 14 observables, which have been derived and listed in Ref. [69]. For the Moravcsik-complete sets with 14 observables, also some examples exist that contain only 2 observables with recoil polarization (apart from R_T^{y0}). Furthermore, interestingly the combinations of shape classes that lie at the heart of the Moravcsik-complete sets with 14 observables are exactly the same combinations as for the minimal complete sets derived in this work (cf. lists in Appendix D of Ref. [69]). In other words, the Moravcsik-complete sets of 14 are derived from the exact same graph-topologies shown in Fig. 10, but using Theorem 2 from Appendix A instead of Theorem 1 from Sec. II. Furthermore, we suspect that many of the 1216 minimal com-

plete sets with 12 observables, which have been derived in this work, are in fact subsets of the Moravcsik-complete sets of 14 from Ref. [69]. In Sec. VI from Ref. [69], this has been illustrated explicitly for the minimal complete set

$$\{\mathcal{O}_{1+}^c, \mathcal{O}_{2-}^c, \mathcal{O}_{2+}^g, \mathcal{O}_{2-}^g, \mathcal{O}_{2+}^h, \mathcal{O}_{2-}^h\}, \quad (49)$$

which is numerated as the set “(c, g, h) : 68” in the lists of the Supplemental Material [83], which result from the calculations performed in the present work. Furthermore, it has been demonstrated explicitly in Ref. [69] how this minimal complete set with 12 observables can be deduced from a Moravcsik-complete set of 14 via a mathematical reduction procedure. We assume that similar facts are true for many more cases, but have not checked all cases explicitly in the course of this work.

When comparing to the statements made on minimal complete sets for electroproduction in the work by Tiator and collaborators [74], we have to state that our findings corroborate their statements. Still, our work complements Ref. [74] by giving an explicit graphical construction procedure for minimal complete sets, which has implied an extensive list of 1216 such sets [83]. Such a graphical procedure was not given in Ref. [74] and neither has been a list of complete sets. However, as a final remark, we recite here a useful alternative construction procedure for complete sets in electroproduction, which has in fact been proposed in Ref. [74]. This alternative procedure consists of combining a complete photoproduction set with one full shape class of electroproduction observables from the four possibilities $\{e, f, g, h\}$. We see that the definitions of the shape classes D1, a, b, and c are algebraically identical to the definitions of the photoproduction observables (compare Tables I and III). Thus, one can take for instance any of the complete sets derived in Sec. III and combine it for example with the full shape class e. This yields then a set of $(8 + 4) = 12$ observables. The four complex amplitudes b_1, \dots, b_4 are determined uniquely up to one overall phase from the complete photoproduction set. The 2 moduli and the 2 relative phases which are missing from just the 8 observables in the complete photoproduction set are then uniquely fixed via the 4 quantities from the shape class e, as has been already pointed out in Ref. [74]. Therefore, this method of combining complete photoproduction sets with a full shape class from $\{e, f, g, h\}$ represents a powerful and elegant alternative scheme for the derivation of complete sets for electroproduction, which is complementary to the approach followed in the present work.

This concludes our discussion of the case (2+2+2) for pseudoscalar meson electroproduction. By this we mean complete sets emerging from selections of three pairs of observables from three different shape classes, based on the 8 start topologies shown in Fig. 10. Although a quite extensive list of 1216 complete sets of minimal length was found this way, we acknowledge that many more such sets exist for electroproduction (cf. statements made in Ref. [74]). We continue our discussion with comments on a possible generalization of the graphical criterion to problems with $N > 6$ amplitudes.

V. GENERALIZATION TO PROBLEMS INVOLVING $N > 6$ AMPLITUDES

In order to provide an idea on how the new graphical criterion proposed in this work can be generalized to processes with larger numbers of $N > 6$ amplitudes, we consider here the next more complicated case of two-meson photoproduction, which is generally described by $N = 8$ amplitudes [76,81]. We do not list here the definitions of all the $N^2 = 64$ polarization observables for two-meson photoproduction, due to reasons of space. Their definitions, as well as an explanation of their physical meaning in terms of actual measurements, can be found in Refs. [76,81]. It is clear that a minimal complete set for two-meson photoproduction has to contain at least $2N = 16$ observables (cf. remarks in the introduction, Sec. I, as well as Ref. [76]).

The general structure encountered in this case is as follows: The 64 observables contain one shape class with 8 diagonal observables, which are capable of uniquely fixing the moduli $|b_1|, \dots, |b_8|$ of the transversity amplitudes. The remaining 56 observables can be grouped into 7 distinct shape classes, containing 8 observables each, which all have the same repeating mathematical structure. For each of the nondiagonal shape classes $n = 1, \dots, 7$, the 8 observables have the following generic form [76]

$$\mathcal{O}_{s1}^n = |b_i||b_j| \sin \phi_{ij} + |b_k||b_l| \sin \phi_{kl} + |b_m||b_p| \sin \phi_{mp} + |b_q||b_r| \sin \phi_{qr}, \quad (50)$$

$$\mathcal{O}_{s2}^n = |b_i||b_j| \sin \phi_{ij} + |b_k||b_l| \sin \phi_{kl} - |b_m||b_p| \sin \phi_{mp} - |b_q||b_r| \sin \phi_{qr}, \quad (51)$$

$$\mathcal{O}_{s3}^n = |b_i||b_j| \sin \phi_{ij} - |b_k||b_l| \sin \phi_{kl} + |b_m||b_p| \sin \phi_{mp} - |b_q||b_r| \sin \phi_{qr}, \quad (52)$$

$$\mathcal{O}_{s4}^n = |b_i||b_j| \sin \phi_{ij} - |b_k||b_l| \sin \phi_{kl} - |b_m||b_p| \sin \phi_{mp} + |b_q||b_r| \sin \phi_{qr}, \quad (53)$$

$$\mathcal{O}_{c1}^n = |b_i||b_j| \cos \phi_{ij} + |b_k||b_l| \cos \phi_{kl} + |b_m||b_p| \cos \phi_{mp} + |b_q||b_r| \cos \phi_{qr}, \quad (54)$$

$$\mathcal{O}_{c2}^n = |b_i||b_j| \cos \phi_{ij} + |b_k||b_l| \cos \phi_{kl} - |b_m||b_p| \cos \phi_{mp} - |b_q||b_r| \cos \phi_{qr}, \quad (55)$$

$$\mathcal{O}_{c3}^n = |b_i||b_j| \cos \phi_{ij} - |b_k||b_l| \cos \phi_{kl} + |b_m||b_p| \cos \phi_{mp} - |b_q||b_r| \cos \phi_{qr}, \quad (56)$$

$$\mathcal{O}_{c4}^n = |b_i||b_j| \cos \phi_{ij} - |b_k||b_l| \cos \phi_{kl} - |b_m||b_p| \cos \phi_{mp} + |b_q||b_r| \cos \phi_{qr}, \quad (57)$$

where the indices $i, j, k, l, m, p, q, r \in 1, \dots, 8$ have to be all pairwise distinct. The 7 nondiagonal shape classes are otherwise only distinguished in the combinations of indices i, j, \dots, r which appear in the above-given definitions. Every shape class composed of 8 observables, which has the structure given above, is in one-to-one correspon-

dence to the particular combination of four relative phases $\{\phi_{ij}, \phi_{kl}, \phi_{mp}, \phi_{qr}\}$. We mention the fact that an algebra of $8 \times 8 \tilde{\Gamma}^\alpha$ matrices is behind the shape class structure shown in Eqs. (50) to (57), as is described in more detail in Ref. [76].

When confronted with a more elaborate structure such as the one given in Eqs. (50) to (57), one can at first make an attempt to reduce the problem to already known cases (cf. Theorems 1 and 2 in Sec. II and Appendix A). Such a reduction can be achieved in the following two ways:

(i) Full decoupling

Considering the definitions of the eight observables in the two-meson photoproduction shape class (50) to (57), one can see quickly that the real and imaginary parts of the bilinear amplitude products, or equivalently the cosines and sines of the corresponding relative phases, can be isolated by defining certain linear combinations of observables. For instance, the sines of the relative phases $\phi_{ij}, \dots, \phi_{qr}$ can be isolated via evaluation of the combinations:

$$|b_i||b_j| \sin \phi_{ij} = \frac{1}{4}(\mathcal{O}_{s1}^n + \mathcal{O}_{s2}^n + \mathcal{O}_{s3}^n + \mathcal{O}_{s4}^n), \quad (58)$$

$$|b_k||b_l| \sin \phi_{kl} = \frac{1}{4}(\mathcal{O}_{s1}^n + \mathcal{O}_{s2}^n - \mathcal{O}_{s3}^n - \mathcal{O}_{s4}^n), \quad (59)$$

$$|b_m||b_p| \sin \phi_{mp} = \frac{1}{4}(\mathcal{O}_{s1}^n - \mathcal{O}_{s2}^n + \mathcal{O}_{s3}^n - \mathcal{O}_{s4}^n), \quad (60)$$

$$|b_q||b_r| \sin \phi_{qr} = \frac{1}{4}(\mathcal{O}_{s1}^n - \mathcal{O}_{s2}^n - \mathcal{O}_{s3}^n + \mathcal{O}_{s4}^n). \quad (61)$$

In exactly the same way, one can isolate the cosines of the relative phases, by defining analogous linear-combinations for the observables $\mathcal{O}_{c1}^n, \dots, \mathcal{O}_{c4}^n$. We say that the bilinear combinations appearing in the original shape class have been *fully decoupled*. In other words, one has reduced the ambiguity-problem provided by the bilinear-forms defined in terms of $8 \times 8 \tilde{\Gamma}^\alpha$ matrices [76] for two-meson photoproduction to the ambiguities implied by certain two-dimensional subalgebras of said $\tilde{\Gamma}^\alpha$ matrices.

It is now possible to apply Moravcsik's theorem in the modified form (Theorem 2 in Appendix A) to the fully decoupled shape class. This has been done in Ref. [76], where complete sets containing at least 24 observables were found using this method.

(ii) Partial decoupling

Instead of trying to isolate the real and imaginary parts of bilinear products alone, one can try to only isolate sub shape classes with four elements, of the same structure as the one given in Eqs. (1) to (4) of Sec. II, which are contained in the 8 observables given above [i.e., in Eqs. (50) to (57)]. For instance, we can find such a subclass, indicated by the symbol $\tilde{\mathcal{O}}^{n,a}$, i.e., with an additional "a" in the superscript, via the following linear combinations of pairs of observables, which contain only the two relative phases ϕ_{ij} and ϕ_{kl} (cf. Ref. [76]):

$$\begin{aligned} \tilde{\mathcal{O}}_{1+}^{n,a} &= \frac{1}{2}(\mathcal{O}_{s1}^n + \mathcal{O}_{s2}^n) \\ &= |b_i||b_j| \sin \phi_{ij} + |b_k||b_l| \sin \phi_{kl}, \end{aligned} \quad (62)$$

$$\begin{aligned}\tilde{\mathcal{O}}_{1-}^{n,a} &= \frac{1}{2}(\mathcal{O}_{s3}^n + \mathcal{O}_{s4}^n) \\ &= |b_i||b_j| \sin \phi_{ij} - |b_k||b_l| \sin \phi_{kl},\end{aligned}\quad (63)$$

$$\begin{aligned}\tilde{\mathcal{O}}_{2+}^{n,a} &= \frac{1}{2}(\mathcal{O}_{c1}^n + \mathcal{O}_{c2}^n) \\ &= |b_i||b_j| \cos \phi_{ij} + |b_k||b_l| \cos \phi_{kl},\end{aligned}\quad (64)$$

$$\begin{aligned}\tilde{\mathcal{O}}_{2-}^{n,a} &= \frac{1}{2}(\mathcal{O}_{c3}^n + \mathcal{O}_{c4}^n) \\ &= |b_i||b_j| \cos \phi_{ij} - |b_k||b_l| \cos \phi_{kl}.\end{aligned}\quad (65)$$

In the same way, one can isolate a subclass $\tilde{\mathcal{O}}^{n,b}$ for the remaining two relative phases ϕ_{mp} and ϕ_{qr} :

$$\begin{aligned}\tilde{\mathcal{O}}_{1+}^{n,b} &= \frac{1}{2}(\mathcal{O}_{s1}^n - \mathcal{O}_{s2}^n) \\ &= |b_m||b_p| \sin \phi_{mp} + |b_q||b_r| \sin \phi_{qr},\end{aligned}\quad (66)$$

$$\begin{aligned}\tilde{\mathcal{O}}_{1-}^{n,b} &= \frac{1}{2}(\mathcal{O}_{s3}^n - \mathcal{O}_{s4}^n) \\ &= |b_m||b_p| \sin \phi_{mp} - |b_q||b_r| \sin \phi_{qr},\end{aligned}\quad (67)$$

$$\begin{aligned}\tilde{\mathcal{O}}_{2+}^{n,b} &= \frac{1}{2}(\mathcal{O}_{c1}^n - \mathcal{O}_{c2}^n) \\ &= |b_m||b_p| \cos \phi_{mp} + |b_q||b_r| \cos \phi_{qr},\end{aligned}\quad (68)$$

$$\begin{aligned}\tilde{\mathcal{O}}_{2-}^{n,b} &= \frac{1}{2}(\mathcal{O}_{c3}^n - \mathcal{O}_{c4}^n) \\ &= |b_m||b_p| \cos \phi_{mp} - |b_q||b_r| \cos \phi_{qr}.\end{aligned}\quad (69)$$

This pair of disjoint subclasses is not the only such pair which can be formed from the eight observables (50) to (57). One can actually split the full shape class into three possible pairs of disjoint subclasses, for which the above-given two (“ n, a ” and “ n, b ”) are just the first example. The second possibility would be given by disjoint shape classes “ n, c ” and “ n, d ” with associated pairs of relative phases $\{\phi_{ij}, \phi_{mp}\}$ and $\{\phi_{kl}, \phi_{qr}\}$, respectively. The precise definitions of the classes “ n, c ” and “ n, d ” then proceed analogously to the Eqs. (62) to (69). Furthermore, one can also form a third combination of disjoint shape classes, we call them “ n, e ” and “ n, f ,” which correspond to the pairs of relative phases $\{\phi_{ij}, \phi_{qr}\}$ and $\{\phi_{kl}, \phi_{mp}\}$, respectively. This exhausts all the possibilities to achieve a partial decoupling of the full shape class shown in Eqs. (50) to (57). We see that some freedom on how to achieve this decoupling indeed exists.

To the partially decoupled shape classes with four elements, such as those described above, our new graphical criterion (Theorem 1 from Sec. II) can be directly applied. Thus, one would search for (2+2+2+2)-combinations selected from four of the partially decoupled shape classes, i.e., four shape classes in the $\tilde{\mathcal{O}}$ basis. However, due to basic topological reasons, it is only possible to derive complete sets with at least 20 observables in this way, when considering observables in the \mathcal{O} basis. This is true due to the fact that at least three shape classes in the \mathcal{O} basis have to be combined in order to get a connected graph when combining the indices from all their relative phases [76]. This means that the above-mentioned (2+2+2+2)-combinations in the $\tilde{\mathcal{O}}$ basis

have to correspond to at least 12 observables in the \mathcal{O} basis. Together with the 8 “diagonal” observables for two-meson photoproduction, this implies 20 observables in total.

Last, we mention the fact that the observables in the partially decoupled shape classes (i.e., in the $\tilde{\mathcal{O}}$ basis) can be used for an explicit algebraic derivation of minimal complete sets of 16 observables in the \mathcal{O} basis, as has been done in Ref. [76]. However, in this derivation, a selection-pattern was used which does not correspond to Theorem 1 from Sec. II.

The approaches (i) and (ii) described above clearly exhaust all the possibilities of directly applying the criteria stated in Sec. II and Appendix A to the problem of two-meson photoproduction. In case one wishes to make statements about more general combinations of observables, one has no other choice but to execute a new dedicated derivation of the general structure of the phase ambiguities allowed by the definitions (50) to (57).

(iii) *Full derivation of new phase-ambiguity structure*

A full dedicated derivation of the phase ambiguities implied by more general selections from a combination of shape classes such as the one defined in Eqs. (50) to (57) has not been performed in the course of this work. Therefore, in the following we can only speculate how such a derivation might look like.

The most nearby option would be to try patterns of (2+2+2+2)-combinations in the \mathcal{O} basis, i.e., selections of 8 nondiagonal observables with 2 observables picked from each individual shape class. These selections do not fit the patterns outlined in point (ii) above. Therefore, some algebraic ingenuity is needed in the derivation and it is likely that trying to exactly replicate the derivation shown in detail in Appendix B might not be enough. Since the derivations from Appendix B are already quite involved, we only expect the new calculations needed for the larger shape classes to be more complicated. However, once the derivation of the discrete phase ambiguities implied by, for instance, the (2+2+2+2)-combinations mentioned above has been completed, we expect that again a graphical criterion similar to the one formulated in Theorem 1 from Sec. II can be used in order to derive complete sets. These complete sets then have the minimal length of $2N = 16$ observables.

The discussion in this section has illustrated the problems which are encountered when trying to generalize the criterion posed in Theorem 1 from Sec. II to more involved problems with $N > 6$ amplitudes. Theorem 1 has been able to directly yield minimal complete sets of length $2N$ for photoproduction and electroproduction, i.e., for $N \leq 6$. Therefore, in these cases it has outperformed the modified form of Moravcsik’s theorem (Theorem 2 from Appendix A). However, the price one has to pay for this achievement is that a simple selection of minimal complete sets for $N > 6$ is not so easily possible. Instead, the advantage of deriving minimal complete sets is paid with new and quite involved algebraic derivations, which

have to be performed for more complicated amplitude extraction problems, with larger and more involved shape classes.

VI. CONCLUSIONS AND OUTLOOK

We have introduced a generalization of the graphs originally introduced by Moravcsik [68], which has led to a new graphical criterion that allows for the determination of minimal complete sets of length $2N$, for an amplitude extraction problem with $N \leq 6$ complex amplitudes, where furthermore N has to be *even*. The new method rests heavily on the known discrete phase ambiguities implied by the selection of any pair of observables from a nondiagonal shape class composed of four quantities. In order to achieve the selection of minimal complete sets for $N \leq 6$, the considered graphs must be provided with additional directional information. Our new criterion has been applied to single-meson photoproduction ($N = 4$ amplitudes) as well as electroproduction ($N = 6$ amplitudes), with success. In particular, we were able to determine for the first time an extensive list of complete sets with minimal length $2N = 12$ for the case of electroproduction.

However, the generalization of our new criterion to problems involving a larger number of $N > 6$ amplitudes is difficult, due to the fact that one has to perform new and more involved algebraic derivations for the ambiguity structure implied by the then appearing larger shape classes, i.e., with more than four observables in each class. It is possible to decouple such a problem, in order to reduce it to the already known case of the above-mentioned shape classes of four. However, the complete sets of observables determined in this way are generally not of minimal length $2N$ any more.

Once the algebraic derivation of the full ambiguity structure allowed by such larger shape classes has been performed successfully, the selection of complete sets according to a graphical criterion similar to the one proposed in this work is straightforward. The derivation of the ambiguity structure is actually the only significant hurdle in the treatment of the more complicated problems. Once this hurdle is taken, graphical criteria can be applied with full effect.

This work can be extended into multiple directions. The obvious first choice would be to work out the new graphical criteria for more complicated reactions with $N > 6$ amplitudes, such as two-meson photoproduction ($N = 8$) or even vector-meson photoproduction ($N = 12$), and to try to extract minimal complete sets with length $2N$ for these reactions. For this, some algebraic ingenuity is needed to treat the larger shape classes. Another possible direction of research would be to try to establish a closer contact to mathematicians, in order to see whether they have deeper insights into the discussed matters. When Moravcsik published his paper in 1985 [68], he called the mathematical theory for the ambiguities of a set of bilinear algebraic equations for several unknowns to be “nonexistent” (see the second-last paragraph in the introduction of Ref. [68]). However, this may have changed in the most recent years and it could be that mathematicians use the objects and approaches introduced in this work, but in different guises. Nevertheless, we have to admit that also the present work seems to lead to a kind of more general theory for the unique solvability of systems of bilinear equations.

ACKNOWLEDGMENTS

The work of Y.W. was supported by the Transdisciplinary Research Area—Building Blocks of Matter and Fundamental Interactions (TRA Matter) during the completion of this paper. The author thanks Philipp Kroenert for useful comments on the paper and for helpful remarks regarding the software needed for the creation of the presented figures.

APPENDIX A: REVIEW OF MORAVCSIK’S THEOREM

This Appendix provides a review of Moravcsik’s theorem [68] in a slightly modified form, which resulted from a recent reexamination [69]. The review is included both to keep the present work self-contained and also because Moravcsik’s theorem serves as a useful reference point to the new graphical criterion, which is developed in Sec. II of the main text.

Consider an amplitude-extraction problem formulated in terms of N complex transversity-amplitudes¹⁰ b_1, \dots, b_N . For such a problem, one can consider the N^2 bilinear amplitude products

$$b_j^* b_i, \quad \text{for } i, j = 1, \dots, N. \quad (\text{A1})$$

Due to the bilinear structure of the products (A1), as well as the fact that polarization observables are most generally linear combinations of such products, the amplitudes generally can only be determined up to one unknown overall phase [52,54,55,73], which can depend on all kinematic variables describing the considered process. Therefore, the maximal amount of information which can be extracted is contained in the moduli and relative phases of the N amplitudes.

An important initial standard assumption is that all the N moduli,

$$|b_1|, |b_2|, \dots, |b_N|, \quad (\text{A2})$$

have already been determined from a suitable subset composed of N “diagonal” observables. This assumption makes the algebraic analysis of complete experiments easier (cf. Refs. [52,68,69,73]) and therefore we shall always adopt it in this paper.

When introducing polar coordinates (i.e., modulus and phase) for each amplitude, the real parts of the generally complex bilinear products become

$$\text{Re}[b_j^* b_i] = |b_i| |b_j| \cos \phi_{ij}. \quad (\text{A3})$$

The real parts thus fix their corresponding relative phase $\phi_{ij} := \phi_i - \phi_j$ up to the discrete ambiguity [68,73]

$$\phi_{ij}^\lambda = \phi_{ij}^\pm = \begin{cases} +\alpha_{ij}, \\ -\alpha_{ij}, \end{cases} \quad (\text{A4})$$

¹⁰One can also formulate all statements made in this work for helicity instead of transversity amplitudes. However, in the transversity basis, the observables which can uniquely fix amplitude moduli are generally most easily measured [52,73,74] (cf. discussions on photoproduction in Sec. III and electroproduction in Sec. IV). Therefore, we have decided to choose the latter basis.

where α_{ij} can be extracted uniquely from the value of $\text{Re}[b_j^* b_i]$, and on the interval $\alpha_{ij} \in [0, \pi]$. We call a discrete ambiguity of the form (A4) a “cosine-type” ambiguity [69].

The imaginary part of a bilinear product is written as

$$\text{Im}[b_j^* b_i] = |b_i| |b_j| \sin \phi_{ij}, \quad (\text{A5})$$

and it yields the corresponding relative phase ϕ_{ij} up to the discrete phase ambiguity [68,73]

$$\phi_{ij}^\lambda = \phi_{ij}^\pm = \begin{cases} +\alpha_{ij}, \\ \pi - \alpha_{ij}, \end{cases}, \quad (\text{A6})$$

where α_{ij} can be extracted uniquely from the quantity $\text{Im}[b_j^* b_i]$, and on the interval $\alpha_{ij} \in [-\pi/2, \pi/2]$. We refer to a discrete ambiguity of the form (A6) as a “sine-type” ambiguity [69].

The original theorem by Moravcsik is formulated as a “geometrical analog” [68]. In this analog, every amplitude is represented by a point and each bilinear amplitude product is thus given as a line connecting the points that correspond to the amplitudes among which the product is taken [cf. Eq. (A1)]. Furthermore, a solid line represents the real part $\text{Re}[b_j^* b_i]$ and a broken (dashed) line denotes the imaginary part $\text{Im}[b_j^* b_i]$.

Moravcsik’s theorem has been recently reexamined [69], which has lead to a slight modification of the original statement. The modified form of Moravcsik’s theorem has then been applied to single-meson photo- and electroproduction [69], and also very recently to two-meson photoproduction [76]. It reads as follows [69]:

Theorem 2 (Modified form of Moravcsik’s theorem):

Consider the following “most economical” [68] situation in the geometrical analog: a large open chain which contains *all* amplitude points and thus consists of $N - 1$ lines for a problem with N amplitudes. This open chain is now turned into a *fully* complete set, by adding one additional connecting line which turns it into a closed loop of N lines, which has to contain all amplitude points exactly once. Furthermore, in such a closed loop every amplitude point is touched by exactly 2 link lines. In other words, we have generated a fully connected graph with N vertices and N edges, where all vertices have to have exactly the order 2.

Such a connected graph (or closed loop) corresponds to a unique solution for the amplitude-extraction problem, which does not permit any residual discrete ambiguities, in case it satisfies the following criterion:

- (C2) The connected graph has to contain an odd number of dashed lines $n_d \geq 1$.

In particular, the graph does not have to contain any solid lines at all. For an odd number of links N , the connected graph with $n_d = N$ therefore still represents a fully complete set.

It is irrelevant which of the bilinear amplitude products are represented by the dashed lines, as long as the overall number of dashed lines is odd.

A detailed proof of this theorem can be found in Appendix A of Ref. [69]. As an illustration of the somewhat abstract criterion formulated in Theorem 2, we show three

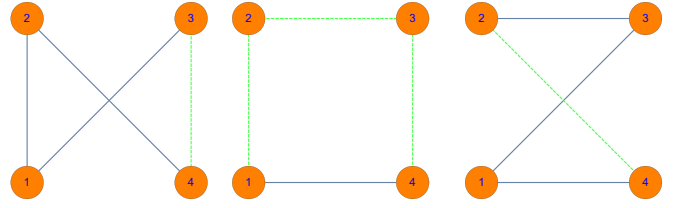


FIG. 14. The diagrams show three connected graphs which meet all the criteria posed by Theorem 2. These graphs with 4 vertices correspond to the well-known example case of pseudoscalar meson photoproduction, which is a problem with $N = 4$ amplitudes. Green dashed lines denote the imaginary part of a bilinear amplitude product, while the real part of such a product is represented by a blue solid line. These graphs have been taken over identically from Ref. [69].

fully complete example graphs for pseudoscalar meson photoproduction ($N = 4$ amplitudes) in Fig. 14. In the following, we comment on some features of the theorem which are important for the present work.

The requirement of a connected topology for the graph considered in Theorem 2 is crucial, due to the fact that it directly forbids combinations of relative phases corresponding to multiple disconnected subsets of amplitudes in the complex plane, where the relative phases among all amplitudes within one subset are uniquely fixed, but the multiple subsets are still allowed to rotate freely relative to each other. The latter case occurs when at least one relative phase connecting at least two such subsets is missing, and it leads to so-called *continuous ambiguities*. The connectedness criterion for the graph directly removes such continuous ambiguities.

Furthermore, in case the connectedness criterion is fulfilled, one can establish a so-called *consistency relation* [69,73] among all the occurring relative phases. The generic form as well as the importance of such consistency relations is elaborated in more detail in the beginning of Sec. II of the main text.

We note that there can exist certain singular surfaces in the parameter space composed of the relative phases, on which Theorem 2 no longer holds. Such singular configurations have been mentioned in Sec. III and Appendix A of Ref. [69]. However, we will disregard such cases in the following discussion, since the measure of such singular surfaces is always negligible, when compared to the full parameter space.

The modified form of Moravcsik’s theorem (i.e., Theorem 2) has turned out to be very useful, since it leads to a fully automated procedure for the construction of complete sets for in principle *any* amplitude extraction problem with a general number of N complex amplitudes. However, when applied to realistic processes with $N \geq 4$ amplitudes, this theorem has lead to sets which are slightly overcomplete when compared to complete sets of minimal length $2N$ (see in particular Sec. VII of Ref. [69], as well as the discussion in Ref. [76]). This happens essentially due to fact that isolated real and imaginary parts of bilinear amplitude products [Eqs. (A3) and (A5)] enter the statement of Theorem 2, while the observables encountered in processes with $N \geq 4$ amplitudes are generally linear combinations of such bilinear products. The new graphical criterion, which is developed in Sec. II of the main text,

represents an attempt to improve this situation by allowing for a direct selection of fully complete sets with minimal length $2N$.

APPENDIX B: DERIVATION OF THE PHASE AMBIGUITIES FOR THE SIMPLEST NONTRIVIAL SHAPE SLASS [Eqs. (1)–(4)]

In the following, we repeat the derivations from Sec. III of Nakayama's work [73]. First, we consider the example case B.1 [selection of $(\mathcal{O}_{1+}^n, \mathcal{O}_{2+}^n)$] mentioned in Sec. II. We define $B_{ij} := |b_i||b_j|$ and consider the following pair of observables:

$$\mathcal{O}_{1+}^n = B_{ij} \sin \phi_{ij} + B_{kl} \sin \phi_{kl}, \quad (\text{B1})$$

$$\mathcal{O}_{2+}^n = B_{ij} \cos \phi_{ij} + B_{kl} \cos \phi_{kl}. \quad (\text{B2})$$

When combining both of these definitions, a basic addition theorem for the cosine leads to the following expression:

$$(\mathcal{O}_{1+}^n)^2 + (\mathcal{O}_{2+}^n)^2 = B_{ij}^2 + B_{kl}^2 + 2B_{ij}B_{kl} \cos(\phi_{ij} - \phi_{kl}). \quad (\text{B3})$$

We define the length

$$N \equiv N_{1+,2+}^n := \sqrt{(\mathcal{O}_{1+}^n)^2 + (\mathcal{O}_{2+}^n)^2}. \quad (\text{B4})$$

Then, we formally introduce the transitional angle $\zeta \equiv \zeta_{1+,2+}^n$ via:

$$\cos \zeta \equiv \frac{\mathcal{O}_{1+}^n}{N}, \quad \sin \zeta \equiv \frac{\mathcal{O}_{2+}^n}{N}. \quad (\text{B5})$$

Compare this definition to the comments made below Eq. (11), as well as to the graphical representation shown in Fig. 2, in Sec. II. One should always keep in mind that the general angle $\zeta_{v\pm, v'\pm}^n$ and the length $N_{v\pm, v'\pm}^n$ both depend on the considered pair of observables.

With these definitions, the observables given above can be re-expressed as

$$N \cos \zeta = B_{ij} \sin \phi_{ij} + B_{kl} \sin \phi_{kl}, \quad (\text{B6})$$

$$N \sin \zeta = B_{ij} \cos \phi_{ij} + B_{kl} \cos \phi_{kl}. \quad (\text{B7})$$

Next, we multiply the first of these equations by $\sin \phi_{kl}$ and the second one by $\cos \phi_{kl}$ and then add both equations, which

leads to:

$$\cos(\phi_{ij} - \phi_{kl}) = \frac{-B_{kl} + N \sin(\zeta + \phi_{kl})}{B_{ij}}. \quad (\text{B8})$$

Inserting this result in Eq. (B3), one obtains:

$$\sin(\zeta + \phi_{kl}) = \frac{N^2 - B_{ij}^2 + B_{kl}^2}{2NB_{kl}}. \quad (\text{B9})$$

Applying the arcsin function to this equation, one can derive the phase ambiguity

$$\phi_{kl} = \begin{cases} -\zeta + \alpha_{kl}, \\ -\zeta - \alpha_{kl} + \pi, \end{cases} \quad (\text{B10})$$

where the right-hand side of Eq. (B9) uniquely fixes α_{kl} on the interval $[-\pi/2, \pi/2]$.

In exactly the same way that has led to Eq. (B9), one can prove the following constraint:

$$\sin(\zeta + \phi_{ij}) = \frac{B_{ij}^2 - B_{kl}^2 + N^2}{2NB_{ij}}. \quad (\text{B11})$$

This constraint leads to the following discrete phase ambiguity:

$$\phi_{ij} = \begin{cases} -\zeta + \alpha_{ij}, \\ -\zeta - \alpha_{ij} + \pi, \end{cases} \quad (\text{B12})$$

where the right-hand side of Eq. (B11) uniquely specifies α_{ij} on the interval $[-\pi/2, \pi/2]$.

Up to now, the discrete phase ambiguity given by Eqs. (B10) and (B12) looks like a fourfold one, but this is not true due to the fact that the relative phases ϕ_{ij} and ϕ_{kl} are *not* independent. Rather, Eq. (B3) fixes a constraint for $\cos(\phi_{ij} - \phi_{kl})$. In other words, one has $\pm\tilde{\alpha} \equiv \phi_{ij} - \phi_{kl}$, where $\tilde{\alpha}$ is uniquely specified on the interval $[0, \pi]$. The ambiguities (B10) and (B12) leave the following four possibilities for the difference of the relative phases:

$$\phi_{ij} - \phi_{kl} = \begin{cases} \alpha_{ij} - \alpha_{kl}, \\ \alpha_{ij} + \alpha_{kl} - \pi, \\ -\alpha_{ij} - \alpha_{kl} + \pi, \\ -\alpha_{ij} + \alpha_{kl}. \end{cases} \quad (\text{B13})$$

After taking out the indeterminacy of the sign of $\pm\tilde{\alpha}$, which is true due to the symmetry of the cosine, one is left with the following set of two nonredundant cases for the quantity $\tilde{\alpha}$:

$$\tilde{\alpha} = \begin{cases} \alpha_{ij} - \alpha_{kl}, \\ \alpha_{ij} + \alpha_{kl} - \pi. \end{cases} \quad (\text{B14})$$

We evaluate the cosine of the second possibility for $\tilde{\alpha}$, as follows:

$$\begin{aligned} \cos(\phi_{ij} - \phi_{kl}) &= \cos(\alpha_{ij} + \alpha_{kl} - \pi) = -\cos \alpha_{ij} \cos \alpha_{kl} + \sin \alpha_{ij} \sin \alpha_{kl} = -\sqrt{(1 - \sin^2 \alpha_{ij})(1 - \sin^2 \alpha_{kl})} + \sin \alpha_{ij} \sin \alpha_{kl} \\ &= -\sqrt{\left(1 - \left[\frac{B_{ij}^2 - B_{kl}^2 + N^2}{2NB_{ij}}\right]^2\right)\left(1 - \left[\frac{N^2 - B_{ij}^2 + B_{kl}^2}{2NB_{kl}}\right]^2\right)} + \frac{B_{ij}^2 - B_{kl}^2 + N^2}{2NB_{ij}} \frac{N^2 - B_{ij}^2 + B_{kl}^2}{2NB_{kl}} \\ &= \frac{N^2 - B_{ij}^2 - B_{kl}^2}{2B_{ij}B_{kl}}. \end{aligned} \quad (\text{B15})$$

The calculation needed to get from the third to the fourth step in Eq. (B15) is quite involved. The numerator of the square-root term becomes the absolute value $|B_{ij}^4 + (B_{kl}^2 - N^2)^2 - 2B_{ij}^2(B_{kl}^2 + N^2)|$. Once we insert the equation for N^2 , i.e., Eq. (B3), into the term within the absolute value, we see that this term equals $-4B_{ij}^2B_{kl}^2 \sin^2(\phi_{ij} - \phi_{kl})$, which is definitely a negative number. Thus, evaluating the absolute value amounts to flipping the sign of this term. Keeping track of this sign change, it is then possible to derive the correct result (B15).

We observe that the second of the two nonredundant possibilities (B14) satisfies the correct constraint (B3) for $\cos(\phi_{ij} - \phi_{kl})$. In exactly the same way as done above, one can check that the first possibility in (B14) leads to an equation which is different from (B3). Thus, we have derived that the difference of the relative phases ϕ_{ij} and ϕ_{kl} always has to satisfy:

$$\phi_{ij} - \phi_{kl} = \pm(\alpha_{ij} + \alpha_{kl} - \pi). \quad (\text{B16})$$

The fact that this relation has to hold reduces the fourfold discrete ambiguity derived initially to a twofold one. The remaining constraint (B16) is only generally fulfilled by the following two cases:

$$\begin{cases} \phi_{ij} = -\zeta + \alpha_{ij}, \\ \phi_{kl} = -\zeta - \alpha_{kl} + \pi, \end{cases} \quad \text{or} \quad \begin{cases} \phi_{ij} = -\zeta - \alpha_{ij} + \pi, \\ \phi_{kl} = -\zeta + \alpha_{kl}. \end{cases} \quad (\text{B17})$$

$$\begin{aligned} \cos(\phi_{ij} - \phi_{kl}) &= \cos(\alpha_{ij} - \alpha_{kl}) = \cos \alpha_{ij} \cos \alpha_{kl} + \sin \alpha_{ij} \sin \alpha_{kl} \\ &= \sqrt{(1 - \sin^2 \alpha_{ij})(1 - \sin^2 \alpha_{kl})} + \sin \alpha_{ij} \sin \alpha_{kl} \\ &= \sqrt{\left(1 - \left[\frac{B_{ij}^2 - B_{kl}^2 + N^2}{2NB_{ij}}\right]^2\right) \left(1 - \left[\frac{-N^2 + B_{ij}^2 - B_{kl}^2}{2NB_{kl}}\right]^2\right)} + \frac{B_{ij}^2 - B_{kl}^2 + N^2}{2NB_{ij}} \frac{-N^2 + B_{ij}^2 - B_{kl}^2}{2NB_{kl}} \\ &= \frac{-N^2 + B_{ij}^2 + B_{kl}^2}{2B_{ij}B_{kl}}. \end{aligned} \quad (\text{B22})$$

The second possibility mentioned in Eq. (B14) leads to the wrong constraint for $\cos(\phi_{ij} - \phi_{kl})$. Therefore, in the case B.4, the following constraint has to hold:

$$\phi_{ij} - \phi_{kl} = \pm(\alpha_{ij} - \alpha_{kl}). \quad (\text{B23})$$

This constraint leaves only the following twofold phase ambiguity for the case B.4:

$$\begin{cases} \phi_{ij} = -\zeta + \alpha_{ij}, \\ \phi_{kl} = -\zeta + \alpha_{kl}, \end{cases} \quad \text{or} \quad \begin{cases} \phi_{ij} = -\zeta - \alpha_{ij} + \pi, \\ \phi_{kl} = -\zeta - \alpha_{kl} + \pi. \end{cases} \quad (\text{B24})$$

Now, we treat the case B.2 from Sec. II, i.e., we consider the following pair of observables:

$$\mathcal{O}_{1+}^n = B_{ij} \sin \phi_{ij} + B_{kl} \sin \phi_{kl}, \quad (\text{B25})$$

$$\mathcal{O}_{2-}^n = B_{ij} \cos \phi_{ij} - B_{kl} \cos \phi_{kl}. \quad (\text{B26})$$

The derivation for this case corresponds to the expressions derived for B.1 above, with both the signs of B_{kl} and ϕ_{kl}

Consider next the case B.4 described in Sec. II, i.e., the combination of observables $(\mathcal{O}_{1-}^n, \mathcal{O}_{2-}^n)$. From their definitions

$$\mathcal{O}_{1-}^n = B_{ij} \sin \phi_{ij} - B_{kl} \sin \phi_{kl}, \quad (\text{B18})$$

$$\mathcal{O}_{2-}^n = B_{ij} \cos \phi_{ij} - B_{kl} \cos \phi_{kl}, \quad (\text{B19})$$

we see that the entire derivation given above for the case B.1 can be mimicked, with the only change needed being a flip of the sign of B_{kl} in every intermediate step. Thus, we can infer the following two constraints:

$$\sin(\zeta + \phi_{kl}) = \frac{-N^2 + B_{ij}^2 - B_{kl}^2}{2NB_{kl}}, \quad (\text{B20})$$

$$\sin(\zeta + \phi_{ij}) = \frac{N^2 + B_{ij}^2 - B_{kl}^2}{2NB_{ij}}. \quad (\text{B21})$$

Applying the arcsin function yields here again an apparent fourfold discrete phase ambiguity, with formally the same expressions as given in Eqs. (B10) and (B12). However, now the derivation (B15) changes. We again consider the two nonredundant cases for the $\tilde{\alpha}$ variable given in Eq. (B14). However, now some quite involved algebra shows that:

flipped. The expression (B3) changes as follows:

$$(\mathcal{O}_{1+}^n)^2 + (\mathcal{O}_{2-}^n)^2 = B_{ij}^2 + B_{kl}^2 - 2B_{ij}B_{kl} \cos(\phi_{ij} + \phi_{kl}). \quad (\text{B27})$$

One has to keep in mind that now the constraint for the cosine holds for $\cos(\phi_{ij} + \phi_{kl})$. Following the derivation further, one obtains the following pair of constraints:

$$\sin(\zeta - \phi_{kl}) = \frac{-N^2 + B_{ij}^2 - B_{kl}^2}{2NB_{kl}}, \quad (\text{B28})$$

$$\sin(\zeta + \phi_{ij}) = \frac{N^2 + B_{ij}^2 - B_{kl}^2}{2NB_{ij}}. \quad (\text{B29})$$

These two constraints fix the relative phases ϕ_{ij} and ϕ_{kl} up to the following discrete ambiguities

$$\phi_{kl} = \begin{cases} \zeta - \alpha_{kl}, \\ \zeta + \alpha_{kl} - \pi, \end{cases} \quad \text{and} \quad \phi_{ij} = \begin{cases} -\zeta + \alpha_{ij}, \\ -\zeta - \alpha_{ij} + \pi. \end{cases} \quad (\text{B30})$$

For the sum of both relative phases, one thus obtains the following four possible cases:

$$\phi_{ij} + \phi_{kl} = \begin{cases} \alpha_{ij} - \alpha_{kl}, \\ \alpha_{ij} + \alpha_{kl} - \pi, \\ -\alpha_{ij} - \alpha_{kl} + \pi, \\ -\alpha_{ij} + \alpha_{kl}. \end{cases} \quad (\text{B31})$$

One again has to single out the nonredundant cases

$$\tilde{\alpha} = \begin{cases} \alpha_{ij} - \alpha_{kl}, \\ \alpha_{ij} + \alpha_{kl} - \pi. \end{cases} \quad (\text{B32})$$

In a calculation which is formally quite similar to (B22), one can check that the correct constraint for $\cos(\phi_{ij} + \phi_{kl})$ is satisfied by:

$$\phi_{ij} + \phi_{kl} = \pm(\alpha_{ij} - \alpha_{kl}). \quad (\text{B33})$$

This relation for the sum of the relative phases singles out the following twofold discrete phase ambiguity for the case B.2:

$$\begin{cases} \phi_{ij} = -\zeta + \alpha_{ij}, \\ \phi_{kl} = \zeta - \alpha_{kl}, \end{cases} \quad \text{or} \quad \begin{cases} \phi_{ij} = -\zeta - \alpha_{ij} + \pi, \\ \phi_{kl} = \zeta + \alpha_{kl} - \pi. \end{cases} \quad (\text{B34})$$

Finally, we consider the case B.3 from Sec. II, i.e., the selection of the following pair of observables:

$$\mathcal{O}_{1-}^n = B_{ij} \sin \phi_{ij} - B_{kl} \sin \phi_{kl}, \quad (\text{B35})$$

$$\mathcal{O}_{2+}^n = B_{ij} \cos \phi_{ij} + B_{kl} \cos \phi_{kl}. \quad (\text{B36})$$

Here, one can follow the steps in the derivation for the case B.1, which has been described above, and only has to flip the sign of the relative phase ϕ_{kl} . Thus, Eq. (B3) turns into:

$$(\mathcal{O}_{1-}^n)^2 + (\mathcal{O}_{2+}^n)^2 = B_{ij}^2 + B_{kl}^2 + 2B_{ij}B_{kl} \cos(\phi_{ij} + \phi_{kl}), \quad (\text{B37})$$

The constraint for the cosine is again valid for the sum of both relative phases ϕ_{ij} and ϕ_{kl} .

For this case B.3, one can derive the following set of constraints:

$$\sin(\zeta - \phi_{kl}) = \frac{N^2 - B_{ij}^2 + B_{kl}^2}{2NB_{kl}}, \quad (\text{B38})$$

$$\sin(\zeta + \phi_{ij}) = \frac{N^2 + B_{ij}^2 - B_{kl}^2}{2NB_{ij}}. \quad (\text{B39})$$

The two relative phases ϕ_{ij} and ϕ_{kl} are thus fixed up to the following discrete ambiguities

$$\phi_{kl} = \begin{cases} \zeta - \alpha_{kl}, \\ \zeta + \alpha_{kl} - \pi, \end{cases} \quad \text{and} \quad \phi_{ij} = \begin{cases} -\zeta + \alpha_{ij}, \\ -\zeta - \alpha_{ij} + \pi. \end{cases} \quad (\text{B40})$$

The thus implied possible cases for the sum $\phi_{ij} + \phi_{kl}$ are formally the same as in Eq. (B31) and the nonredundant cases for the quantity $\tilde{\alpha}$ are formally the same as in Eq. (B32).

One has again to be careful with the constraint for $\cos(\phi_{ij} + \phi_{kl})$. In a calculation which is formally similar to the steps taken in (B15), one can deduce that for the case B.3, the following constraint has to hold:

$$\phi_{ij} + \phi_{kl} = \pm(\alpha_{ij} + \alpha_{kl} - \pi). \quad (\text{B41})$$

This relation singles out the following twofold discrete phase ambiguity for the case B.3:

$$\begin{cases} \phi_{ij} = -\zeta + \alpha_{ij}, \\ \phi_{kl} = \zeta + \alpha_{kl} - \pi, \end{cases} \quad \text{or} \quad \begin{cases} \phi_{ij} = -\zeta - \alpha_{ij} + \pi, \\ \phi_{kl} = \zeta - \alpha_{kl}. \end{cases} \quad (\text{B42})$$

APPENDIX C: DISCRETE PHASE AMBIGUITIES OF THE SIMPLEST NONTRIVIAL SHAPE CLASS [Eqs (1)–(4)] FOR COMBINATIONS OF OBSERVABLES WITH FLIPPED SIGNS

In this Appendix, we derive the discrete phase ambiguities for observables selected from the shape class given in Eqs. (1)–(4) in Sec. II, provided that at least one of the observables has a flipped sign. We will see that this leads to more general combinations of signs for the ζ angles in the ambiguity-formulas (more general compared to those listed in Sec. II). Although this derivation yields in principle redundant information, the obtained results are still useful in case one wishes to derive complete sets starting solely from considerations of graphs, as discussed in more detail in Sec. III. The results derived in the following have been collected in Table II of the main text.

The first and simplest way of deriving the phase ambiguities for combinations of observables with flipped signs proceeds via consideration of Eq. (B5) from Appendix B. Suppose we reverse the sign of the second observable in this formula, i.e., we consider the observables $(\mathcal{O}_{1+}^n, -\mathcal{O}_{2+}^n)$. Then, Eq. (B5) becomes

$$\cos \zeta \equiv \frac{\mathcal{O}_{1+}^n}{N}, \quad \sin \zeta \equiv \frac{-\mathcal{O}_{2+}^n}{N}. \quad (\text{C1})$$

Suppose now that another angle, called ‘ $\tilde{\zeta}$ ’, exists for which the equation retains its original form:

$$\cos \tilde{\zeta} \equiv \frac{\mathcal{O}_{1+}^n}{N}, \quad \sin \tilde{\zeta} \equiv \frac{\mathcal{O}_{2+}^n}{N}. \quad (\text{C2})$$

Then, we have

$$\cos \tilde{\zeta} = \cos \zeta, \quad \text{and} \quad \sin \tilde{\zeta} = -\sin \zeta, \quad (\text{C3})$$

or

$$\tilde{\zeta} = -\zeta. \quad (\text{C4})$$

We see that the ζ angle has reversed its sign when going from $(\mathcal{O}_{1+}^n, \mathcal{O}_{2+}^n)$ to $(\mathcal{O}_{1+}^n, -\mathcal{O}_{2+}^n)$. This can also be seen via consideration of Fig. 2.

Alternatively, consider now the combination $(-\mathcal{O}_{1+}^n, \mathcal{O}_{2+}^n)$, which leads to the following equations:

$$\cos \zeta \equiv \frac{-\mathcal{O}_{1+}^n}{N}, \quad \sin \zeta \equiv \frac{\mathcal{O}_{2+}^n}{N}. \quad (\text{C5})$$

In the same way as before, one derives for this case:

$$\tilde{\zeta} = \pi - \zeta. \quad (\text{C6})$$

An additional summand of π appears now in the ambiguity-formulas, which is however irrelevant. The important point is that also in this case, the sign of the ζ angle has been reversed. In exactly the same way, one can show that for the combination $(-\mathcal{O}_{1+}^n, -\mathcal{O}_{2+}^n)$, the ζ angle retains its original sign.

The second possible way of deriving the ambiguities for flipped signs of observables proceeds by going through the steps for case B.1 as discussed in Appendix B. However, this time we flip the sign of the first observable: $(-\mathcal{O}_{1+}^n, \mathcal{O}_{2+}^n)$. Considering the definitions in Eqs. (B1) and (B2), we observe that flipping the sign of \mathcal{O}_{1+}^n is tantamount to reversing the signs of both relative phases ϕ_{ij} and ϕ_{kl} . Following the derivation through, we obtain the following constraints:

$$\sin(\zeta - \phi_{kl}) = \frac{N^2 - B_{ij}^2 + B_{kl}^2}{2NB_{kl}}. \quad (\text{C7})$$

$$\sin(\zeta - \phi_{ij}) = \frac{B_{ij}^2 - B_{kl}^2 + N^2}{2NB_{ij}}. \quad (\text{C8})$$

These two constraints directly imply the following discrete phase ambiguities:

$$\phi_{kl} = \begin{cases} \zeta - \alpha_{kl}, \\ \zeta + \alpha_{kl} - \pi, \end{cases} \quad \text{and} \quad \phi_{ij} = \begin{cases} \zeta - \alpha_{ij}, \\ \zeta + \alpha_{ij} - \pi. \end{cases} \quad (\text{C9})$$

We see that from then on the ζ 's appear with reversed signs in all formulas compared to the original derivation for case

B.1, given in Appendix B (cf. Eqs. (B10) and (B12)). The same is true when one considers the combination with the sign of the second observable flipped: $(\mathcal{O}_{1+}^n, -\mathcal{O}_{2+}^n)$. The latter case can be obtained from the original derivation for B.1 by reversing the signs of all the quantities ϕ_{ij} , ϕ_{kl} , B_{ij} , and B_{kl} [cf. Eqs. (B1) and (B2)]. However, in case one would consider the combination $(-\mathcal{O}_{1+}^n, -\mathcal{O}_{2+}^n)$, all one would have to do is reverse the signs of the modulus factors B_{ij} and B_{kl} , which would leave the signs of the ζ angles in the ambiguity formulas untouched.

By repeating the arguments given above for the case 'B.4' considered in Appendix B, one can derive the remaining associations between the ζ -sign combinations “ $(-\zeta, -\zeta)$ ” and “ $(+\zeta, +\zeta)$ ” and specific pairs of observables, which are given in Table II of the main text.

Finally, in order to obtain all the associations of pairs of observables to the ζ -sign combinations “ $(-\zeta, +\zeta)$ ” and “ $(+\zeta, -\zeta)$,” one has to repeat the steps described above for the cases B.2 and B.3 discussed in Appendix B. In this way, the full set of associations given in Table II is obtained.

-
- [1] E. Klempt and J. M. Richard, *Rev. Mod. Phys.* **82**, 1095 (2010).
[2] D. G. Ireland, E. Pasyuk, and I. Strakovsky, *Prog. Part. Nucl. Phys.* **111**, 103752 (2020).
[3] A. Thiel *et al.*, *Phys. Rev. Lett.* **109**, 102001 (2012).
[4] M. Gottschall *et al.*, *Phys. Rev. Lett.* **112**, 012003 (2014).
[5] J. Hartmann *et al.*, *Phys. Rev. Lett.* **113**, 062001 (2014).
[6] N. Sparks *et al.*, *Phys. Rev. C* **81**, 065210 (2010).
[7] F. Afzal *et al.*, *Phys. Rev. Lett.* **125**, 152002 (2020).
[8] F. Afzal, *EPJ Web Conf.* **241**, 01001 (2020).
[9] M. Dugger *et al.*, *Phys. Rev. C* **88**, 065203 (2013).
[10] P. Collins *et al.*, *Phys. Lett. B* **771**, 213 (2017).
[11] I. Senderovich *et al.*, *Phys. Lett. B* **755**, 64 (2016).
[12] S. Strauch *et al.*, *Phys. Lett. B* **750**, 53 (2015).
[13] P. T. Mattione *et al.*, *Phys. Rev. C* **96**, 035204 (2017).
[14] D. Ho *et al.*, *Phys. Rev. Lett.* **118**, 242002 (2017).
[15] M. C. Kunkel *et al.*, *Phys. Rev. C* **98**, 015207 (2018).
[16] D. Hornidge *et al.*, *Phys. Rev. Lett.* **111**, 062004 (2013).
[17] M. H. Sikora *et al.*, *Phys. Rev. Lett.* **112**, 022501 (2014).
[18] S. Schumann *et al.* (MAINZ-A2 Collaboration), *Phys. Lett. B* **750**, 252 (2015).
[19] P. Adlarson *et al.*, *Phys. Rev. C* **92**, 024617 (2015).
[20] S. Gardner *et al.*, *Eur. Phys. J. A* **52**, 333 (2016).
[21] J. Annand *et al.*, *Phys. Rev. C* **93**, 055209 (2016).
[22] V. L. Kashevarov *et al.* (A2 Collaboration), *Phys. Rev. Lett.* **118**, 212001 (2017).
[23] M. Dieterle *et al.*, *Phys. Lett. B* **770**, 523 (2017).
[24] W. Briscoe *et al.*, *Phys. Rev. C* **100**, 065205 (2019).
[25] H. Kohri *et al.*, *Phys. Rev. C* **97**, 015205 (2018).
[26] H. Kohri, *EPJ Web Conf.* **241**, 01010 (2020).
[27] H. Al Ghouli *et al.*, *Phys. Rev. C* **95**, 042201 (2017).
[28] S. Adhikari *et al.*, *Phys. Rev. C* **100**, 052201 (2019).
[29] S. Adhikari *et al.*, *Nucl. Instrum. Methods A* **987**, 164807 (2021).
[30] V. D. Burkert (CLAS Collaboration), *EPJ Web Conf.* **134**, 01001 (2017).
[31] N. Markov *et al.*, *Phys. Rev. C* **101**, 015208 (2020).
[32] V. D. Burkert, *EPJ Web Conf.* **241**, 01004 (2020).
[33] V. Burkert *et al.*, *Nucl. Instrum. Methods A* **959**, 163419 (2020).
[34] R. L. Workman *et al.*, SAID Partial Wave Analysis, <http://gwdac.phys.gwu.edu/>.
[35] R. A. Arndt, R. L. Workman, and M. M. Pavan, *Phys. Rev. C* **49**, 2729 (1994).
[36] R. A. Arndt, I. I. Strakovsky, R. L. Workman, and M. M. Pavan, *Phys. Rev. C* **52**, 2120 (1995).
[37] R. A. Arndt, W. J. Briscoe, I. I. Strakovsky, and R. L. Workman, *Phys. Rev. C* **74**, 045205 (2006).
[38] R. L. Workman, R. A. Arndt, W. J. Briscoe, M. W. Paris, and I. I. Strakovsky, *Phys. Rev. C* **86**, 035202 (2012).
[39] A. Sarantsev *et al.*, Bonn-Gatchina Partial Wave Analysis, <https://pwa.hiskp.uni-bonn.de/>.
[40] A. V. Anisovich *et al.*, *Mesons and Baryons: Systematization and Methods of Analysis* (World Scientific, Singapore, 2009).
[41] A. V. Anisovich, R. Beck, E. Klempt, V. A. Nikonov, A. V. Sarantsev, and U. Thoma, *Eur. Phys. J. A* **48**, 15 (2012).
[42] A. Sarantsev, *Int. J. Mod. Phys.: Conf. Ser.* **26**, 1460081 (2014).
[43] D. Ronchen, M. Doring, F. Huang, H. Habertzettl, J. Haidenbauer, C. Hanhart, S. Krewald, U.-G. Meißner, and K. Nakayama, *Eur. Phys. J. A* **49**, 44 (2013).
[44] D. Rönchen, M. Döring, F. Huang, H. Habertzettl, J. Haidenbauer, C. Hanhart, S. Krewald, U.-G. Meißner, and K. Nakayama, *Eur. Phys. J. A* **50**, 101 (2014).
[45] D. Rönchen, M. Döring, H. Habertzettl, J. Haidenbauer, U.-G. Meißner, and K. Nakayama, *Eur. Phys. J. A* **51**, 70 (2015).
[46] D. Rönchen, M. Döring, and U.-G. Meißner, *Eur. Phys. J. A* **54**, 110 (2018).
[47] M. Mai, M. Döring, C. Granados, H. Habertzettl, U.-G. Meißner, D. Rönchen, I. Strakovsky, and R. Workman (Jülich-Bonn-Washington Collaboration), *Phys. Rev. C* **103**, 065204 (2021).
[48] L. Tiator *et al.*, MAID Partial Wave Analysis, <https://maid.kph.uni-mainz.de/>.
[49] D. Drechsel, S. S. Kamalov, and L. Tiator, *Eur. Phys. J. A* **34**, 69 (2007).

- [50] L. Tiator, M. Gorchtein, V. L. Kashevarov, K. Nikonov, M. Ostrick, M. Hadžimehmedović, R. Omerović, H. Osmanović, J. Stahov and A. Švarc, *Eur. Phys. J. A* **54**, 210 (2018).
- [51] L. Tiator, *Few-Body Syst.* **59**, 21 (2018).
- [52] W. T. Chiang and F. Tabakin, *Phys. Rev. C* **55**, 2054 (1997).
- [53] R. J. Eden, P. V. Landshoff, D. I. Olive, and J. C. Polkinghorne, *The analytic S-matrix* (Cambridge University Press, Cambridge, UK, 1966).
- [54] Y. Wunderlich, Diploma thesis, University of Bonn, 2012.
- [55] Y. Wunderlich, Ph.D. thesis, University of Bonn, 2019.
- [56] M. L. Goldberger, H. W. Lewis, and K. M. Watson, *Phys. Rev.* **132**, 2764 (1963).
- [57] I. P. Ivanov, *Phys. Rev. D* **85**, 076001 (2012).
- [58] R. G. Newton, *J. Math. Phys.* **9**, 2050 (1968).
- [59] A. Martin, *Nuovo Cimento A* **59**, 131 (1969).
- [60] D. Atkinson, P. W. Johnson, and R. L. Warnock, *Commun. Math. Phys.* **28**, 133 (1972).
- [61] C. Itzykson and A. Martin, *Nuovo Cimento A* **17**, 245 (1973).
- [62] D. Atkinson, G. Mahoux, and F. J. Yndurain, *Nucl. Phys. B* **54**, 263 (1973).
- [63] D. Atkinson, G. Mahoux, and F. J. Yndurain, *Nucl. Phys. B* **98**, 521 (1975).
- [64] J. E. Bowcock and H. Burkhardt, *Rep. Prog. Phys.* **38**, 1099 (1975).
- [65] K. Chadan and P. C. Sabatier, *Inverse Problems in Quantum Scattering Theory* (Springer, Berlin, 1977).
- [66] A. Martin and J. M. Richard, *Phys. Rev. D* **101**, 094014 (2020).
- [67] I. S. Barker, A. Donnachie, and J. K. Storrow, *Nucl. Phys. B* **95**, 347 (1975).
- [68] M. J. Moravcsik, *J. Math. Phys.* **26**, 211 (1985).
- [69] Y. Wunderlich, P. Kroenert, F. Afzal, and A. Thiel, *Phys. Rev. C* **102**, 034605 (2020).
- [70] G. Keaton and R. Workman, *Phys. Rev. C* **54**, 1437 (1996).
- [71] G. Keaton and R. Workman, *Phys. Rev. C* **53**, 1434 (1996).
- [72] A. V. Anisovich, R. Beck, E. Klempt, V. A. Nikonov, A. V. Sarantsev, U. Thoma, and Y. Wunderlich, *Eur. Phys. J. A* **49**, 121 (2013).
- [73] K. Nakayama, *Phys. Rev. C* **100**, 035208 (2019).
- [74] L. Tiator, R. L. Workman, Y. Wunderlich, and H. Habertzettl, *Phys. Rev. C* **96**, 025210 (2017).
- [75] H. Arenhövel and A. Fix, *Phys. Rev. C* **89**, 034003 (2014).
- [76] P. Kroenert, Y. Wunderlich, F. Afzal, and A. Thiel, *Phys. Rev. C* **103**, 014607 (2021).
- [77] D. G. Ireland, *Phys. Rev. C* **82**, 025204 (2010).
- [78] T. Vrancx, J. Ryckebusch, T. Van Cuyck, and P. Vancraeyveld, *Phys. Rev. C* **87**, 055205 (2013).
- [79] T. Vrancx, J. Ryckebusch, and J. Nys, *EPJ Web Conf.* **73**, 04011 (2014).
- [80] J. Nys, T. Vrancx, and J. Ryckebusch, *J. Phys. G* **42**, 034016 (2015).
- [81] W. Roberts and T. Oed, *Phys. Rev. C* **71**, 055201 (2005).
- [82] M. Pichowsky, C. Savkli, and F. Tabakin, *Phys. Rev. C* **53**, 593 (1996).
- [83] See Supplemental Material at <http://link.aps.org/supplemental/10.1103/PhysRevC.104.045203> for listings of all complete sets evaluated in Secs. III and IV.
- [84] Wolfram Research, Inc., Mathematica, Version 12.0, Champaign, IL (2019).